Cement and Concrete Research 163 (2023) 107011

Contents lists available at ScienceDirect

Cement and Concrete Research

journal homepage: www.elsevier.com/locate/cemconres

Investigation of leaching in steel fiber-reinforced shotcrete exposed to fresh and saline groundwater in a subsea road tunnel

Cristobal Javier Manquehual [a,*], Pål Drevland Jakobsen [b], Karl Gunnar Holter [b], Klaartje De Weerdt [c], Amund Bruland [a]

[a] Department of Civil and Environmental Engineering, Norwegian University of Science and Technology (NTNU), Trondheim, Norway
[b] Norwegian Geotechnical Institute (NGI), Oslo, Norway
[c] Department of Structural Engineering, Norwegian University of Science and Technology (NTNU), Trondheim, Norway

ARTICLE INFO

Keywords:
Permanent shotcrete
Leaching
TGA
μ-XRF
XRD
Sprayed concrete
Degradation

ABSTRACT

The field and laboratory investigations performed in the Frøya subsea road tunnel, constructed between 1998 and 2000, focus on the degree of leaching undergone by steel fiber-reinforced shotcrete in fresh and saline groundwater. Shotcrete samples were extracted by core drilling at two locations: in the middle of the tunnel approximately 150 m below sea level, and near one of the portals. Leaching is only evident in the first location identified by portlandite reduction, potassium reduction, shotcrete density reduction, and suction porosity increase towards the traffic room. The leached depth is approximately 9 cm.

1. Introduction

The durability of concrete infrastructure is becoming increasingly important due to higher safety standards, higher rehabilitation costs, and a growing concern on sustainability [1–4]. Shotcrete, or sprayed concrete, has been widely used for permanent rock support in tunnels as a single shell lining in several northern European countries and Australia for many years [5]. In particular, the experience with steel fiber-reinforced shotcrete in subsea road tunnels in Norway exceeds 30 years [6]. Shotcrete enables a quick application of rock support, as no formwork is required [7]. The wet-mix process has been systematically used for this purpose. To be sprayable, the wet-mix incorporates only small aggregate particles to prevent blockage of the hose and nozzle and reduce rebound after hitting the substrate. These smaller aggregate particles (common practice in Norway in the 1990s <16 mm) and the addition of an accelerator, which usually has negative consequences in the long-term of the concrete [8], lead to shotcrete requiring a higher amount of cement in comparison to conventional concrete [5]. These differences make the durability investigation results on conventional concrete doubtful when extrapolated to shotcrete [9].

There are laboratory investigations in the literature aimed at evaluating the resistance of shotcrete against aggressive agents by accelerated testing methods [8,10–12]. However, these types of accelerated tests generally focus on specific degradation mechanisms, with samples being exposed to aggressive agents at constant concentrations for a restricted time period.

On the other hand, investigations of on-site shotcrete conditions exposed to simultaneous degradation mechanisms interacting with each other for a long period of time are limited in the literature. Furthermore, in the case of shotcrete installed in road tunnels, one has to bear in mind that its inspection usually involves the interruption of the traffic.

In this research, the leaching level experienced by steel fiber-reinforced shotcrete applied with the wet-mix process in the Frøya subsea road tunnel [13] is investigated at two locations with different environments for the shotcrete. One of these locations lies in the middle of the tunnel where the shotcrete is exposed to saline groundwater. The other location, near one of the portals, the shotcrete is exposed to fresh groundwater. It is important to emphasize that the shotcrete technology and age are, for practical purposes, the same in both locations.

A hydraulic gradient towards the traffic room caused by a groundwater level above the tunnel alignment might promote water percolation through the shotcrete layer. This effect favors the leaching firstly of alkali-metals as they are mainly present in the pore solution due to their low binding capacity to the hydrated cement phases [14]. The first alkali-metal ions to leave the concrete layer will be those located at the downstream end of the percolated water [15]. Locally, the lower content

* Corresponding author.
E-mail address: cristobal.j.manquehual@ntnu.no (C.J. Manquehual).

https://doi.org/10.1016/j.cemconres.2022.107011
Received 16 June 2022; Received in revised form 2 October 2022; Accepted 14 October 2022

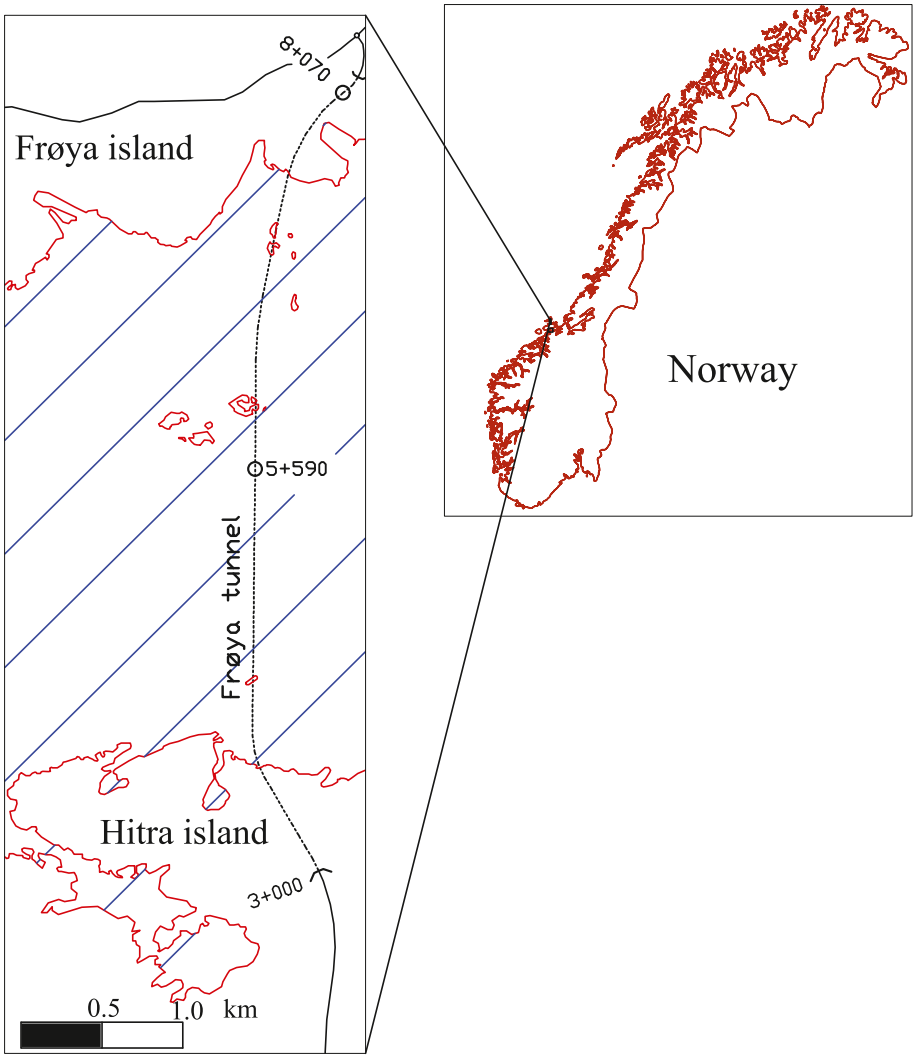

Fig. 1. Top view of the Frøya tunnel, highlighting the two tunnel locations investigated.

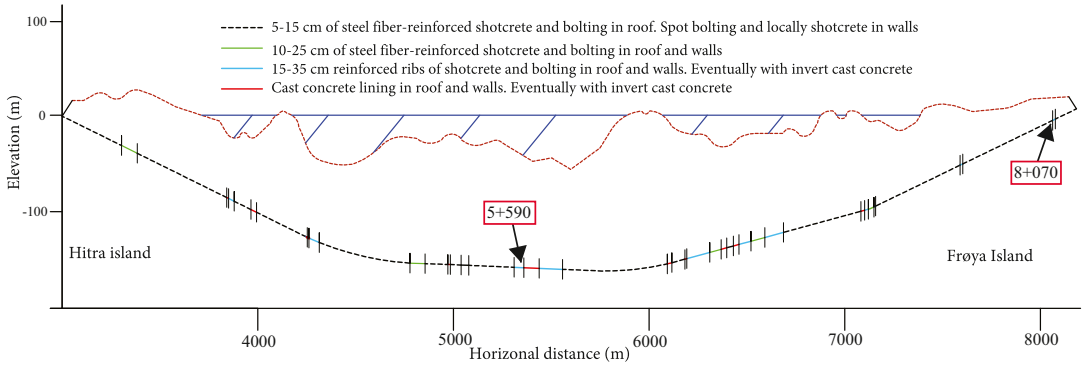

Fig. 2. Longitudinal profile of the Frøya tunnel with the distribution of rock support. The two locations investigated are also highlighted. Modified from [13].

of alkali-metals will trigger a disequilibrium in the pore solution, leading to lower its pH value [16]. The lower alkalinity in the pore solution will increase the solubility of different hydrated cement phases. In particular, portlandite is very sensitive to the pH of pore solution, starting to become unstable when the pH is below 13 [17]. Following the concentration gradient of alkali-metals, it is expected that leaching of the cement paste will initiate on the shotcrete surface exposed to the traffic room (henceforth shotcrete surface) and propagate into the interior of the layer [18]. Leaching will increase the porosity of the cement paste, facilitating the movement of ions, and therefore, promoting further leaching [18].

It is documented in the literature that the presence of chloride ions increases the dissolution of hydrated cement phases [17,19,20]. On the other hand, the more extended the leaching, the deeper the penetration of the chloride ions [21]. In a subsea tunnel, saline groundwater with high concentration of chlorides can reach the shotcrete surface by

Table 1
Wet-mix design in the shotcrete used in the Frøya tunnel with alkali-free accelerator [22].

Aggregate 0–10 mm	1530	kg/m^3
Norcem Standard Cement CEM I «*c*»	475	kg/m^3
Silica fume «*s*»	33	kg/m^3
Alkali-free accelerator (SA 161)	33	kg/m^3
Superplasticizer	1.8	kg/m^3
Internal curing	5	kg/m^3
Dramix steel fiber	44	kg/m^3
Water «*w*»	216	kg/m^3
w/(c + 2 s)	0.40	

Table 2
Field information related to the locations investigated and the cores extracted.

Chainage	5 + 590 (Mid-tunnel)	8 + 070 (Near portal)
Shotcrete core label	1–3; 9–10	4–8
Core length	22–25[a] (cm)	22–38 (cm)
Core diameter	1–3 (55 mm) 9–10 (84 mm)	4 (55 mm) 5–8 (84 mm)
Comments during drilling	None of the cores recovered rock	All the cores recovered rock
Shotcrete surface condition	Wet	Dry
Groundwater pH[b,c]	8.43	8.26
Electrical conductivity of groundwater EC (mS/cm)[b,d]	12.8 (saline)	0.84 (fresh)
Calcium ions Ca^{2+} in groundwater (mg/l)[b,e]	1400	9

[a] Technical problems happened during the drilling of core 3, making it shorter than the neighboring cores (See Fig. 6).
[b] Dripping groundwater coming from the tunnel roof collected in a plastic cup.
[c] The pH measurement was performed with the instrument Laquatwin pH 33, Horiba.
[d] The measurement of the water conductivity was performed with the instrument Laquatwin-EC-33, Horiba.
[e] The measurement of calcium ion concentration was performed with the instrument Laquatwin-Ca-11, Horiba.

percolating the whole shotcrete layer. Similarly, saline groundwater can find pathways of least resistance in the shotcrete layer, such as cracks, at a higher point in the tunnel, and then runs off the shotcrete surface. Chloride ions entering the hardened cement paste in the shotcrete can chemically bind to the AFm phases, forming Friedel's salt or Kuzel's salt [21]. For the sake of simplicity in this research, the term Friedel's salt has been used to describe the more general chloride containing AFm phases.

De-icing salts used during winter times may also play a role in the leaching of the shotcrete layer since its chloride content might be dispersed all over the tunnel by the traffic flow [22].

The shotcrete layer under study is also in contact with atmospheric carbon dioxide since this layer was installed as a single shell, facilitating its carbonation [23]. Alike leaching, carbonation would also propagate from the shotcrete surface, and would also lead to a reduction of the pH in the pore solution [24]. Nevertheless, carbonation also triggers the formation of the calcite mineral which can increase the concrete density, and could potentially inhibit further leaching [25].

Finally, the sulfur present in the pore solution might promote the dissolution of hydrated cement phases which foster further leaching [20]. In a subsea road tunnel, sulfates from the saline groundwater [26], sulfur dioxide gas emitted by vehicles combusting fuel [27,28] and aluminum sulfate in the alkali-free accelerator [29,30] are envisaged as possible sulfur sources.

This research aims to provide field evidence of leaching severity in shotcrete conditions exposed to saline and fresh groundwater. Leaching is investigated using chemical, physical and mechanical tests. This approach might allow to relate the chemical changes found in the cement paste at a microscopic level with macroscopic physical properties and mechanical behavior.

In the laboratory, the shotcrete cores were investigated chemically by Micro-X-ray fluorescence (μ-XRF), thermogravimetric analysis (TGA), X-ray diffraction (XRD) and thymolphthalein pH indicator. The physical properties were investigated by profiles of shotcrete density and suction porosity along different cores. Finally, the mechanical behavior of shotcrete was assessed through the Uniaxial Compressive Strength (UCS) test with axial deformation measurement.

2. Materials and methods

2.1. The Frøya subsea road tunnel

The Frøya tunnel belongs to the connection project of the Hitra, Frøya and Fjellværøy islands with the mainland of Norway. The tunnel length is 5.2 km (from chainage 3 + 000 to chainage 8 + 200) and the lowest level is 164 m below the sea level [31]. Fig. 1 shows a top view of this tunnel, while Fig. 2 shows its longitudinal profile with the distribution of rock support.

The tunnel was excavated in metamorphic rock, with transitions between granitic gneiss, mica-gneiss and migmatite. Several weakness zones found during the tunnel excavation are related to the Tarva fault, which contains soil-like material with swelling potential [32]. During construction, swelling pressure measurements in this material exceeded 1.0 MPa in one specific case [13].

The shotcrete specifications used in this tunnel, constructed between 1998 and 2000, is presented in Table 1.

The required compressive strength for shotcrete installed in subsea

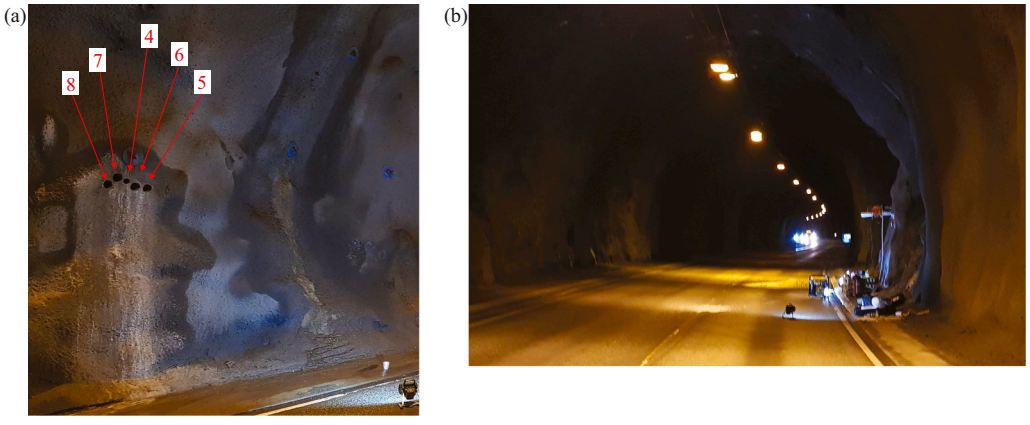

Fig. 3. Investigated location in the Frøya tunnel near the north portal at chainage 8 + 070. (a) Five shotcrete cores already extracted with the corresponding shotcrete label, and (b) wall mounted drilling equipment.

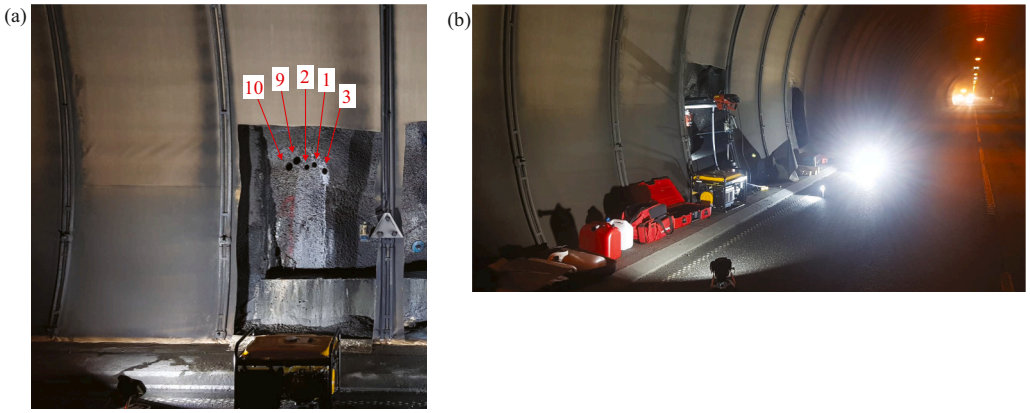

Fig. 4. Investigated location in the Frøya tunnel in the middle of the tunnel at chainage 5 + 590. (a) Five shotcrete cores already extracted with the corresponding shotcrete label, and (b) wall mounted drilling equipment.

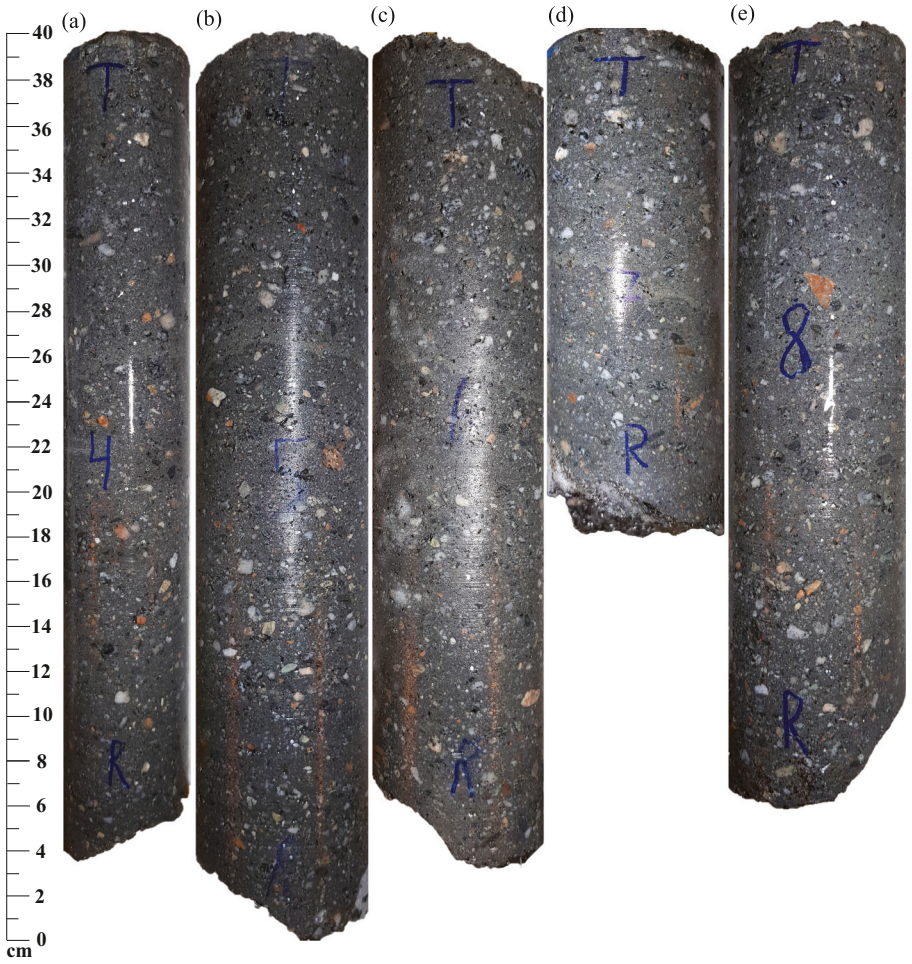

Fig. 5. Cores extracted from chainage 8 + 070 (near portal). From left to right: (a) Core 4, (b) core 5, (c) core 6, (d) core 7, and (e) core 8.

road tunnels at that time was C45 [33]. The equivalent C45 strength required for cylindrical cores extracted from the field was 28.8 MPa according to the valid Norwegian sprayed concrete guidelines at that time [34].

The shotcrete in the Frøya tunnel was installed in contact with the rock as a single shell. Apart from this lining, a Giertsen tunnel water drip protection system consisting of a suspended sheet membrane was installed in large portions of the tunnel. However, this waterproof membrane does not prevent the investigated shotcrete from being exposed to the atmospheric conditions of the traffic room as this membrane is placed 40–60 cm away from the rock support surface.

The selection of the two investigated locations sought to find different environmental conditions for the steel fiber-reinforced shotcrete installed in the Frøya tunnel. One investigated area is located approximately 120 m away from the north portal at chainage 8 + 070, where fresh groundwater was expected (see Figs. 1–2). The second area is located approximately in the middle of the tunnel at chainage 5 + 590, adjacent to a tunnel stretch with cast-in-place concrete lining. The

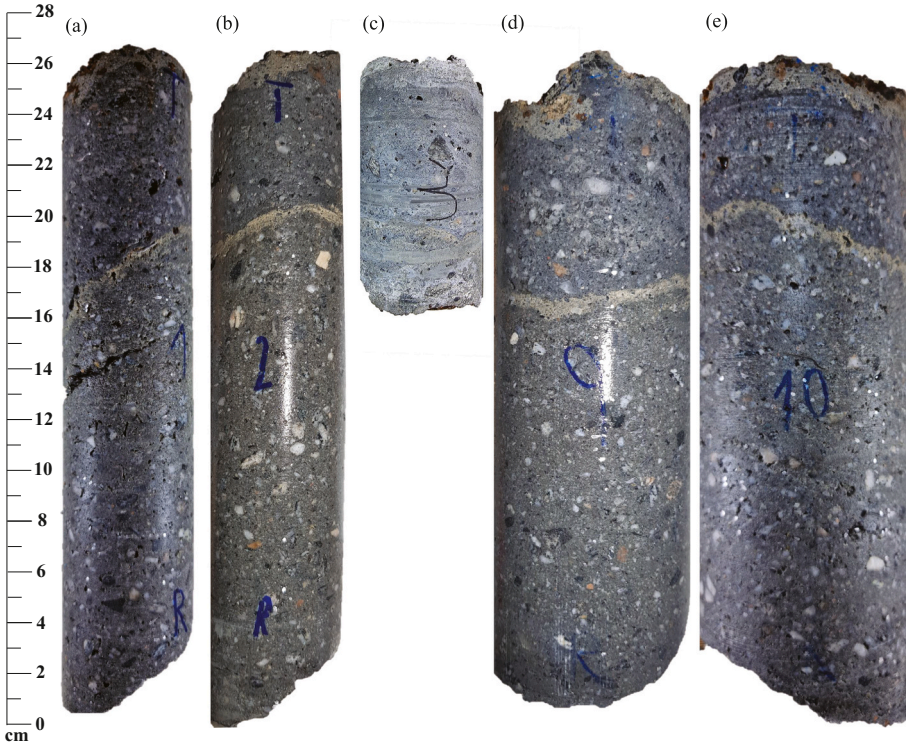

Fig. 6. Cores extracted from chainage 5 + 590 (mid-tunnel). From left to right: (a) Core 1, (b) core 2, (c) core 3, (d) core 9, and (e) core 10.

tunnel inspection occurred on the night of August 30–31 and September 1, 2021. The diamond coring machine was the Hilti DD 150-U. The core bits were 62 and 92 mm in diameter. The resulting shotcrete core diameters were approximately 55 mm and 84 mm respectively. Water was used while drilling to cool the core drill bit and leave a dust-free concrete surface for further drilling. Immediately after the shotcrete cores were extracted from the tunnel walls, they were marked, photographed and tightly wrapped with plastic foil and bubble wrap. Table 2 shows the information obtained in the field for each investigated location.

The groundwater collected near the north portal at chainage 8 + 070 shows low electrical conductivity, indicating that the shotcrete installed in that location is exposed to fresh groundwater. On the other hand, the high electrical conductivity found in the percolated water collected at chainage 5 + 590 indicates that the groundwater is saline. In addition, the calcium ions held in the water collected at chainage 5 + 590 is remarkable. Considering that the calcium ion concentration in sea water lies in the order of 400 mg/l [35,36], the water chemistry at chainage 5 + 590 indicates a significant extra source of calcium in the order of 1000 mg/l after percolating the shotcrete layer.

Figs. 3 and 4 show some images taken at the two locations investigated in the Frøya tunnel.

It is important to highlight that the Giertsen tunnel water drip protection was installed in the investigated location at chainage 5 + 590 (Fig. 4). Figs. 5 and 6 illustrate the cores extracted at chainage 8 + 070 (near portal) and 5 + 590 (mid-tunnel) respectively.

2.2. Methods

2.2.1. pH indicator

One of the consequences of carbonation is the reduction of the pH in the pore solution of the cement paste. In this research, thymolphthalein test method was used to measure the carbonation depth. The thymolphthalein highlights with a bluish tint the surface of concrete samples exceeding a pH of 10.5 [37]. Otherwise, thymolphthalein does not stain the concrete surface. Considering that the pore solution in carbonated concrete can reach a pH value below 9 [25], the non-carbonated area could be distinguished by this pH indicator.

The solution sprayed consisted of 1 g of thymolphthalein dissolved in 70 ml of ethyl alcohol and 30 ml of deionized water.

The tip of core 6 adjacent to the traffic room and core 2 were investigated with this pH indicator. Immediately after unwrapping these two shotcrete cores, they were split along their longitudinal axis to obtain a fresh shotcrete surface. Little cooling water was used while slicing the cores longitudinally with the diamond blade. Only one of the two longitudinal halves of each core was sprayed with thymolphthalein in order to use the second half in other tests. The samples were photographed before and after they were sprayed with the prepared solution.

2.2.2. μ-XRF elemental mapping

The 2D area scanning for sulfur, potassium and chlorine elements in the outermost 15 cm towards the traffic room was investigated with μ-XRF analysis. The μ-XRF scanner utilized was an M4 Tornado from Bruker. The resulting map of a sample shows the fluorescence radiation of the different chemical elements present, and their intensity is related to the number of atoms (concentration) [38]. The corresponding scale of a scan ranges from 0 to 100, being the latter value the highest intensity found in that specific scan. It is important to highlight that no calibration was performed.

Instantly after unwrapping the cores 2, 4 and 9 from the bubble wrap and plastic foil, the cores were split into two halves along their longitudinal axis to obtain fresh, flat surfaces. As in the pH indicator test, a little of cooling water was used while the cores were sliced lengthwise with the concrete saw. Subsequent polishing was not performed. Prior to performing the μ-XRF scanner, the concrete surfaces of the different samples were dried using an air compressor.

The M4 Tornado was used with a silver X-ray tube and only one of the two SDD detectors available. The scanner was run with a step width of 50 μm, a time per pixel of 2 ms, a beam voltage of 50 kV, a tube current of 600 μA, and a pressure in the chamber of 20 mbar.

2.2.3. XRD

The target with powder X-ray diffraction (XRD) analysis was the

Table 3
Investigation techniques performed in this research.

Investigation technique	Degradation mechanism	Expected observation
Chemical analysis		
XRD	Carbonation	Calcite
	Dissolution of cement paste (promoting leaching)/due to Chloride ingress	Friedel's salt
	Possibility of sulfate attack	Ettringite/gypsum/thaumasite
TGA	Leaching (possibly interacting with other degradation mechanisms)	Portlandite content reduction
	Carbonation	Loss of water bound to cement paste above 600 °C
	Dissolution of cement paste (promoting leaching)/due to chloride ingress	Changes in dehydration level between 150 °C - 200 °C and 250 °C – 400 °C (AFm alteration)
	Indication of ettringite enrichment	Large and narrow peaks at 100 °C in DTG curve
pH indicator	Carbonation	Lower pH with the absence of a blueish color
μ-XRF	Dissolution of cement paste (promoting leaching)	Higher content of Chlorine and Sulfur
	Leaching	Reduction of potassium content along the core
	Sulfur enrichment. Possibility of sulfate attack	Higher content of Sulfur
Physical analysis		
Suction porosity	Leaching (possibly interacting with other degradation mechanisms)	Increase in suction porosity
Density	Leaching (possibly interacting with other degradation mechanisms)	Density reduction
Mechanical analysis		
UCS with axial deformation	Leaching (possibly interacting with other degradation mechanisms)	Lower strength with ductile post-peak behavior

identification of secondary minerals present in the cement paste belonging to singularities of the shotcrete layer. That is to say, to identify minerals near the shotcrete surface and at the contact between two shotcrete layers. Cores 1 and 4 were selected for XRD. The database considered for the identification of the minerals was the PDF-4+ 2021 from the International Centre for Diffraction data.

Once cores 1 and 4 were unwrapped, the selection of bulk samples for XRD analysis was achieved by slicing the target zone of the core with a concrete saw. Thereafter, the bulk samples were crushed in a fly press machine to a maximum particle size of approximately 2 mm. In the resulting crushed material, a selective removal of steel fibers and single aggregate particles was performed to obtain a better representation of the cement paste in the XRD sample. The crushing continued with a disc mill to get a particle size of about 50 μm. To reach a maximum particle size of approximately 10 μm, a McCrone micronizing mill was used after the disc mill. The D8 Advance from Bruker was the diffractometer used, which was equipped with a cobalt anode Co-Kα (1.79 Å). The operating parameters used were a Bragg angle ranging from 3° to 80° (2θ), a step size of 0.01°, and a time per step of 0.6 s.

2.2.4. TGA

To investigate in detail the potential leaching at chainage 5 + 590 (mid-tunnel), a profile of the portlandite content was determined using thermogravimetric analysis (TGA) along the same half core (core 2) as the one analyzed in μ-XRF. This half core was sliced crosswise every 10 mm in the 5 cm closest to the traffic room. After this 5 cm, the core was sliced crosswise each 20 mm until a distance of 170 mm away from the

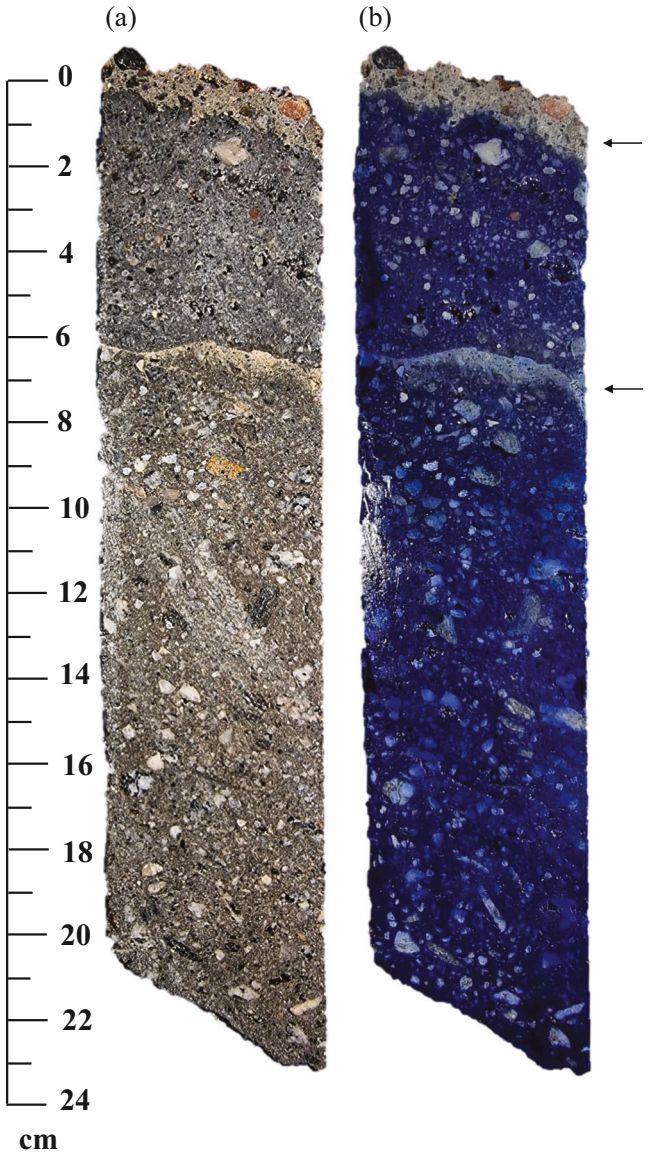

Fig. 7. Thymolphthalein sprayed on half of core 2 split lengthwise. (a) Before application, and (b) after application.

shotcrete surface. The eleven samples obtained were milled, by crushing the sliced samples in a disc mill. The TGA instrument used was a Mettler Toledo TGA/DSC 3^{+}. Approximately 300 mg from each sample was poured into corundum crucibles of 600 μl. The samples were heated from 40 °C to 950 °C at a rate of 10 °C/min, purging the oven with 50 ml/min of nitrogen. The sample weight and the temperature are recorded systematically to create a TG-curve. The loss of water bound to the portlandite occurs approximately at 460 °C [39], but the exact temperature range was determined by analyzing the derivative of the TG-curve (DTG) for each sample. To determine the mass loss of water from the portlandite in each sample, an integration of the DTG curve was calculated between the initial and final temperatures where portlandite decomposes. These temperatures are named in Eq. (1) as T_i and T_f respectively. The portlandite content in each sample was normalized to the dry weight of concrete as described in Eq. (1), where w_{900} represents the sample weight at 900 °C, and $M(portlandite)$ and $M(water)$ represent the molar masses of portlandite and water respectively.

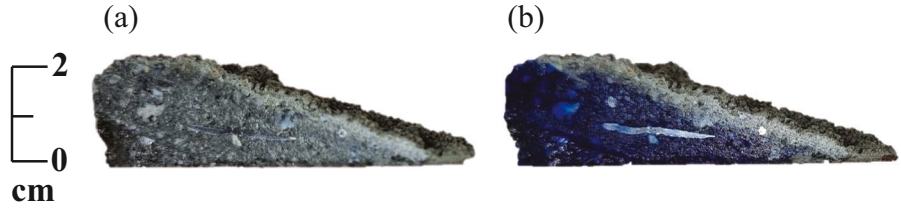

Fig. 8. Thymolphthalein sprayed on the end of the core 6 towards the traffic room split lengthwise. (a) Before application, and (b) after application.

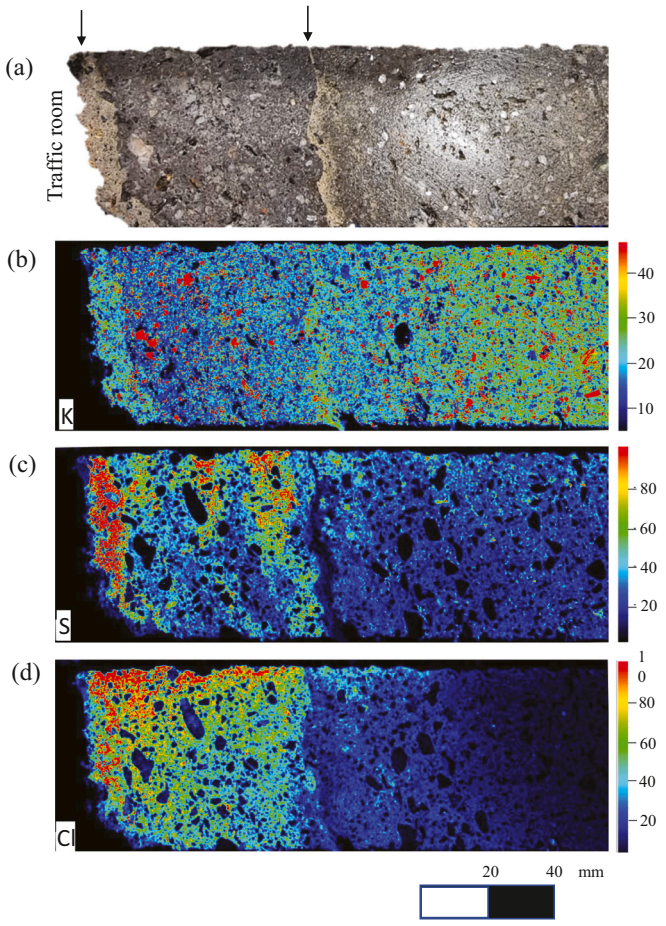

Fig. 9. μ-XRF results in core 2 at chainage 5 + 590 (middle of the tunnel): (a) One half of the shotcrete core split along its longitudinal axis, (b) potassium, (c) sulfur, and (d) chlorine mapping along the core.

$$\text{Portlandite content (wt\%/g dry concrete)} = \frac{\int_{T_i}^{T_f} \text{DTG}}{w_{900}} \cdot \frac{M(portlandite)}{M(water)} \quad (1)$$

In addition, a DTG curve can provide some insights about the level of carbonation. The calcite starts to decompose at temperatures higher than 600 °C. When it comes to sulfur compounds identification in a DTG curve, a narrow curvature with a peak at approximately 100 °C is an indication of ettringite formation [39]. Finally, the decomposition of the AFm phase is related to the weight loss between 150 °C and 200 °C and between 250 °C and 400 °C [21,39].

2.2.5. Suction porosity

The suction porosity test on concrete by immersion was determined following the SINTEF procedure KS 70110 [40]. Basically, the test consists of drying the sample at 105 °C, and then submerge it in water for seven days.

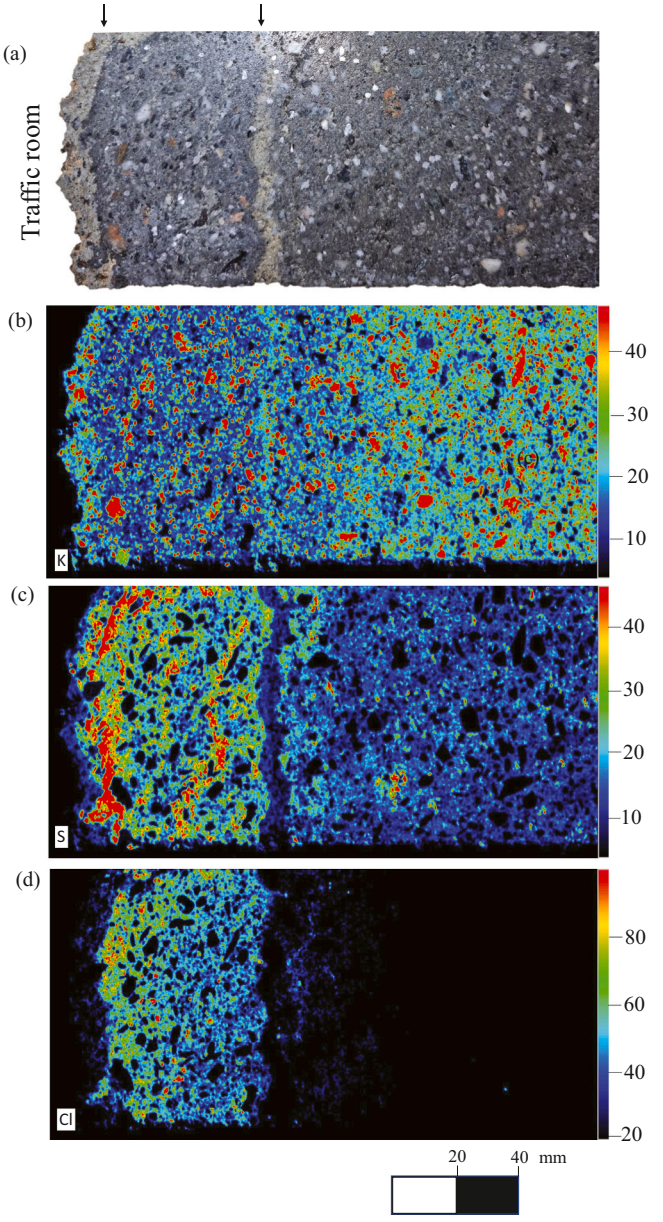

Fig. 10. μ-XRF results in core 9 at chainage 5 + 590 (middle of the tunnel): (a) One half of the shotcrete core split along its longitudinal axis, (b) potassium, (c) sulfur, and (d) chlorine mapping along the core.

The core diameter sets the sample diameter for this test. The cores were sliced crosswise each 20 mm following [40], except for the samples located at the ends of the shotcrete layer in the core, where two parallel

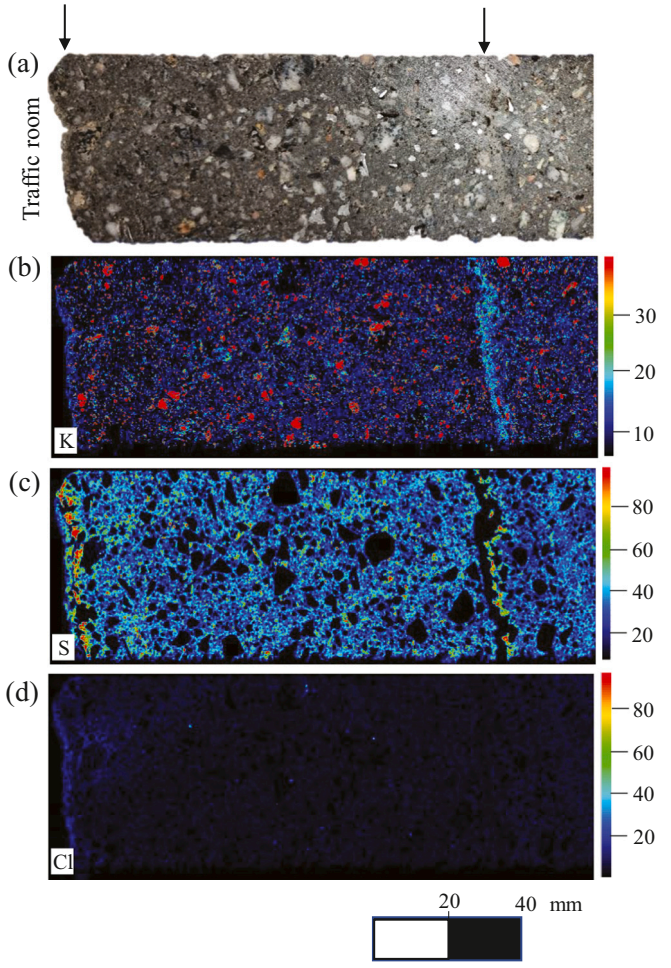

Fig. 11. μ-XRF results in core 4 at chainage 8 + 070 near the north portal: (a) One half of the shotcrete core split along its longitudinal axis, (b) potassium, (c) sulfur, and (d) chlorine mapping along the core.

flat surfaces are not possible to obtain. Cores 5, 7 and 9 were used for this test. They are all 84 mm in diameter. In the specific case of core 9, it was firstly sliced longitudinally along its axis. Only one-half of this core was designated for the suction porosity test, being sliced crosswise each 20 mm as well.

Suction porosity p_s is determined by Eq. (2):

$$p_s = \frac{W_2 - W_1}{W_2 - W_2'} \tag{2}$$

where W_1 is the oven-dry weight of the sample, W_2 is the sample's weight in air after total immersion in water for seven days, and W_2' is the apparent weight of the sample in water, also after water immersion for seven days. A Mettler PC4400 was the balance used in the laboratory.

2.2.6. UCS with axial strain measurements

Eight UCS tests were performed with the Triaxial Testing Systems GCTS RTRX-140CL9. As in the samples for suction porosity, the sample diameter for UCS tests is also fixed by the shotcrete core diameter. In order to get two UCS samples from the same shotcrete core, most of the samples were shorter than the typical height-to-diameter ratio (h/D) of 2.0. The latter h/D value is usually required in standards for concrete specimens, such as NS-EN 12390-1:2012 [41]. Nevertheless, those shorter samples were homologized to a h/D ratio of 2.0 according to the Norwegian standard NS 3420:1986 [42]. This standard establishes a correction factor of 0.96 for a h/D equal to 1.50, and a correction factor of 0.87 for a h/D equal to 1.0.

Cores 1, 6, 8 and 10 were used for this test. After unwrapping these cores in the laboratory, they were immersed in water for seven days before being used for the UCS test. In each UCS test, vertical strain measurements were also performed. To see the response of the different samples after the peak load has been reached, a strain-controlled loading behavior was selected. The strain rate applied varied for each sample, but always in the range of 30 and 50 με/s, trying to fulfill the equivalent loading rate of 0.6 ± 0.2 MPa/s established in standard NS-EN 12390-3:2019 [43] for the compressive strength of hardened concrete. The sensor used to measure the vertical displacement had a theoretical accuracy of 0.001 mm.

2.2.7. Shotcrete density

In this research, the shotcrete density in all cases corresponds to the weight of the samples after total immersion in water for seven days [40]. The volume of suction porosity samples was estimated by the buoyancy method as given in Eq. (3).

$$V = \frac{W_2 - W_2'}{\rho_w} \tag{3}$$

where ρ_w is the water density.

In the case of the cylindrical samples assigned for the UCS test, the sample volume was estimated with a digital caliper according to the ISRM standard [44].

A summary of the investigation techniques performed are given in Table 3.

3. Results

3.1. Chemical investigation techniques

Figs. 7 and 8 show pH indicator results with thymolphthalein in cores 2 and 6 respectively.

Fig. 7 shows a carbonation depth originated from the shotcrete surface of approximately 1.0 cm at chainage 5 + 590 (in the middle of the tunnel). It is interesting to highlight that a second layer of carbonation is indicated in this figure approximately 7.0 cm away from the shotcrete surface.

Fig. 8 indicates that the carbonation depth near the north portal is only a few millimeters. It is remarkable that in Figs. 7 and 8 the zone with lower pH can already be distinguished in the original image before thymolphthalein application by its brownish color compared to the non-carbonated grayish color of the cement paste.

Figs. 9 and 10 show μ-XRF results in cores 2 and 9, both extracted from the middle of the tunnel at chainage 5 + 590.

Figs. 9 and 10 show consistent results in the shotcrete cores extracted at chainage 5 + 590. The three main observations from these two figures are:

- Two brownish layers are shown in Figs. 9a and 10a, one at the shotcrete surface and the other approximately 7 cm away from the shotcrete surface.
- A gradual decay in potassium concentration towards the traffic room is observed in the outermost 9 cm of the shotcrete layer (Figs. 9b and 10b). The exceptions to this trend are the two brownish layers already described with higher local potassium content.
- Sulfur ingress shown in Figs. 9c and 10c overlap with chlorine ingress illustrated in Figs. 9d and 10d in the outermost 7 cm of the shotcrete layer.

Figs. 7 and 8 have already linked the brownish shotcrete layers with zones of lower pH values. The fact that potassium profiles in Figs. 9b and 10b also highlight these two brownish layers is not intuitive, particularly for the ones originated from the shotcrete surface where alkali-metals have probably been leached out in addition to the lower pH detected.

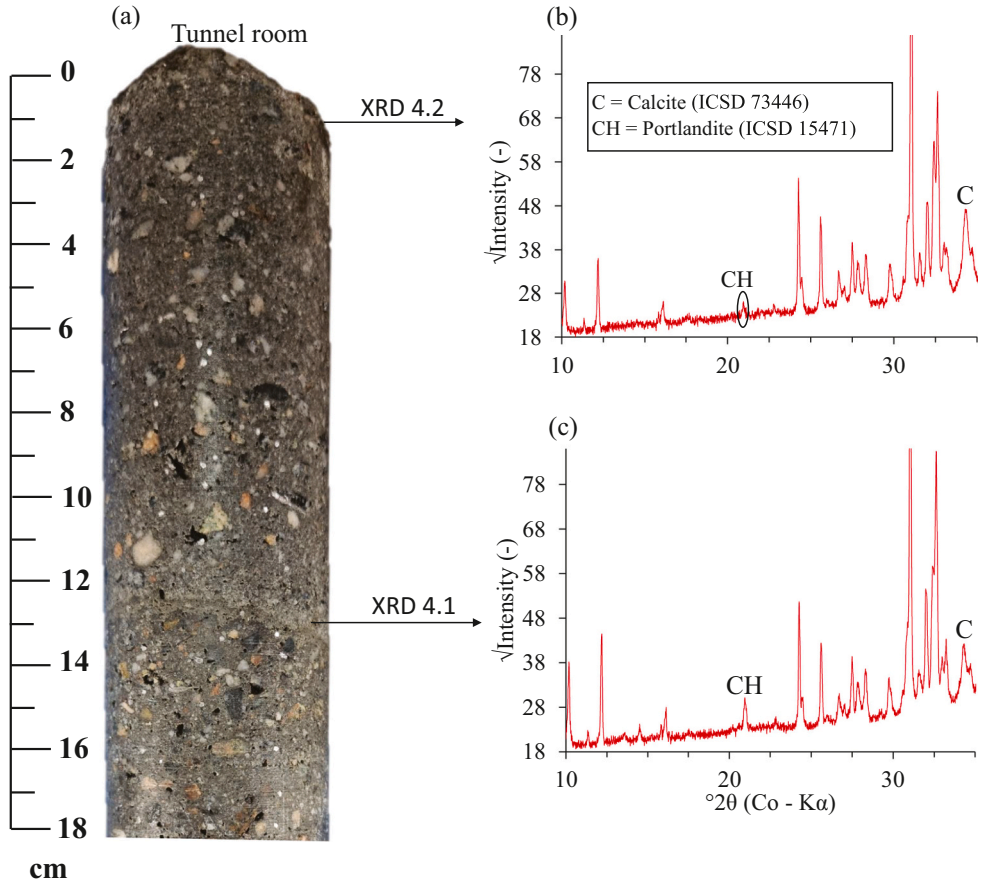

Fig. 12. XRD results in shotcrete layers belonging to core 4 at chainage 8 + 070 (near the north portal) (a) Shotcrete core, (b) XRD analysis at the shotcrete surface, and (c) XRD result at a layer approximately 12 cm away from the shotcrete surface.

However, it has been reported that hydrous silica gel, formed as a decalcification of C-S-H, has the ability to absorb alkali-metals [21,24].

Fig. 10d shows a sudden decay in the chlorine content in these brownish layers. This is consistent with previous observations stating that chloride compounds decompose by either a lower pH or the decalcification of the C-S-H phase [45,46]. In Fig. 9d, the chlorine reduction is only observed at the layer 7 cm inwards from the shotcrete surface.

Alike chlorine, Figs. 9c and 10c show a sudden decay in sulfur in these layers, being more evident in the second layer 7 cm away from the shotcrete surface. In this regard, it is reported that ettringite is unstable at Ph < 10.7 and monosulfate with a pH below 11.6 [47]. The pH value in these shotcrete layers is below 10.5 according to the thymolphthalein pH indicator results, and therefore, ettringite and monosulfate are not stable.

Finally, the reduction in the sulfur and chlorine contents from the shotcrete surface indicates that the source of both elements come from the traffic room.

The μ-XRF results of core 4 extracted from the location near the north portal at chainage 8 + 070 is shown in Fig. 11.

Compared to Figs. 9 and 10, Fig. 11 shows no potassium gradient along core 4 (Fig. 11b), and limited sulfur and chloride ingress from the traffic room (Fig. 11c and d respectively). Alike Figs. 9b and 10b, Fig. 11b also shows two layers of higher potassium content, one at the shotcrete surface and the other approximately 12 cm away from the shotcrete surface. The arrows in Fig. 11a aim to indicate the two layers already described. Fig. 11c shows a sudden sulfur decay in areas of higher potassium, being more evident in the latter layer.

Apart from a lower pH, another indication of carbonation in concrete is the formation of the calcite mineral. Fig. 12 shows XRD results in these shotcrete layers.

The XRD analyses shown in Fig. 12 indicate that shotcrete exposed to the traffic room and at the shotcrete joint, calcite was present. This finding reinforces previous indications that these layers were carbonated. Based on the intensities described in Fig. 12b and c, it is inferred that the degree of carbonation is higher at the shotcrete surface, with a higher calcite intensity and lower portlandite intensity compared to the second layer 12 cm away from the traffic room.

XRD analyses were also performed in core 1, to see if chlorine or sulfur ingress has altered the hydrated cement phases. The results are given in Fig. 13.

Fig. 13b shows that the sample XRD 1.2 exposed to the traffic room has a much higher intensity for the calcite mineral compared to sample XRD 1.1 shown in Fig. 13c. Moreover, the sample XRD 1.2 did not show the presence of portlandite, making more evident that the carbonation level is higher in sample XRD 1.2 in comparison to XRD 1.1. The XRD analyses in XRD 1.2 and XRD 1.1 detected Friedel's salt, a mineral that confirms the presence of chloride ions. In this regard, it is important to highlight the higher intensity of the Friedel's salt in sample XRD 1.1 compared to sample XRD 1.2. In Fig. 13, sulfur compounds such as ettringite, thaumasite or gypsum were not found, despite higher sulfur content found in this area of the shotcrete layer shown in Figs. 9c and 10c. Note that XRD results belonging to the investigated location near the north portal shown in Fig. 12 detected neither sulfur nor chlorine compounds.

The gradual reduction of potassium towards the traffic room shown in Figs. 9b and 10b are indications of leaching at chainage 5 + 590 (in the middle of the tunnel). To study leaching in more detail in this investigated location, a profile of portlandite content in core 2 is shown in Fig. 14 based on TGA results.

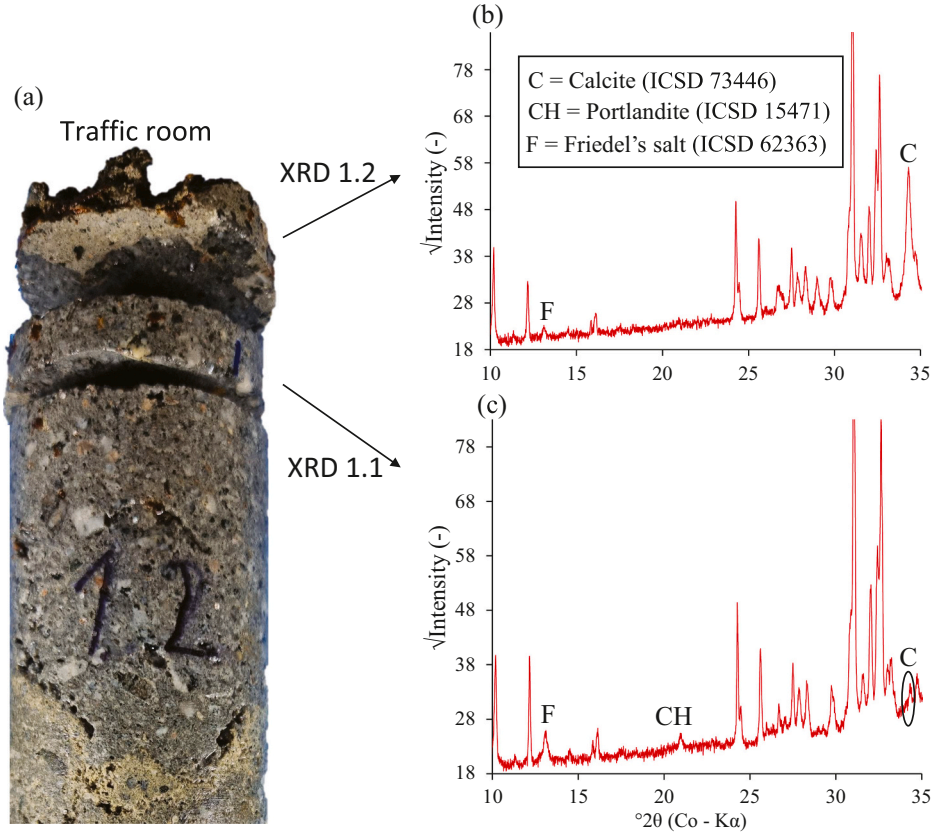

Fig. 13. XRD results at the top of core 1 towards the traffic room (a) Shotcrete core, (b) XRD 1.2 sample at the shotcrete surface, and (c) XRD 1.1 sample adjacent to the carbonation zone.

Fig. 14 clearly shows a reduction in the portlandite content towards the traffic room. A local lower value between 5 and 7 cm away from the shotcrete surface is probably related to a carbonation layer as suggested by Fig. 7 with a lower pH value. It is interesting to highlight as well that the average portlandite content in the 9 cm closest to the shotcrete surface is approximately 0.5 wt% dry concrete. This is approximately the zone in the shotcrete layer where Figs. 9b and 10b illustrate a potassium concentration decay. On the other hand, farther away in the shotcrete layer, the average portlandite content is approximately 1.55 wt% dry concrete. This second zone in the shotcrete layer does not illustrate visible potassium decay. Based on these figures, it is deducted that the portlandite content was reduced, on average, by 68 % in the 9 cm closest to the shotcrete surface.

Fig. 15 shows the DTG curve for each section shown in Fig. 14.

DTG curves illustrated in Fig. 15 show that the largest calcite peaks and thereby highest calcite content in core 2 are in the outermost 20 mm of the shotcrete layer (samples "0–1 cm" and "1–2 cm"). Another section with a noticeable calcite content occurs between 5 and 7 cm away from the shotcrete surface. This zone in the core, also studied with a pH indicator (Fig. 7), turned out to have a lower pH. Thus, Fig. 15 reinforces the indication that the brownish shotcrete layer located 6.5 cm away from the shotcrete surface is carbonated.

The large DTG peak with its maximum at about 110–125 °C can be associated with the decomposition of ettringite [39]. Fig. 15a shows that the ettringite peak becomes slightly larger and broader moving towards the traffic room, indicating a slight increase in the ettringite content. The "5-7 cm" section has the highest ettringite content. It is important to mention that some ettringite is expected along the core since Portland cement and alkali-free accelerator were used [48]. The outermost "0–1 cm" section in Fig. 15b does not show a clear ettringite peak, which can be expected as ettringite is not stable at the lower pH of this carbonated section. Fig. 15b also shows that between 10 mm and 50 mm away from the shotcrete surface, the ettringite content is similar to the innermost sample "15–17 cm". A higher ettringite content was expected in the outermost 7 cm as the sulfur maps shown in Figs. 9c and 10c indicated a higher sulfur content in the outermost 7 cm of the shotcrete layer. The reason for this discrepancy is unclear. Sulfur in cement paste can be bound in ettringite, but can also be adsorbed by C-S-H. Potentially the higher sulfur content is due to adsorption by the C-S-H phase [49].

The DTG peaks observed in the temperature range between 150 °C and 200 °C and between 250 °C and 400 °C, in Fig. 15, are associated with the decomposition of AFm phases. In particular, between 250 °C and 400 °C, a double weight loss peak can be observed in the samples lying between 10 and 70 mm away from the shotcrete surface. This double peak has been related to chloride containing AFm, e.g. Friedel's salt [21]. The observation of the weight loss peaks associated with chloride containing AFm between 10 mm and 70 mm away from the shotcrete surface is consistent with the chloride penetration observed in Figs. 9d and 10d using μ-XRF, as well as identification of Friedel's salt by XRD in Fig. 13. Note that the AFm phases do not seem to be stable in the outmost carbonated "0–1 cm" section, as expected.

3.2. Physical and mechanical investigation techniques

Fig. 16 shows suction porosity and density results in core 9 extracted from the middle of the tunnel at chainage 5 + 590.

Note in Fig. 16b and c that there is a tendency of higher suction porosity and lower density values towards the traffic room. In fact, the samples 9.1, 9.2 and 9.3 have a suction porosity close to 20 % and a density of approximately 2290 kg/m^3, while the three samples closest to the traffic room 9.5, 9.6 and 9.7 have a suction porosity close to 23 % and a density of 2230 kg/m^3. The transition between these two zones occurs in sample 9.4 approximately 9 cm away from the traffic l room. In the same figure, samples 9.5 and 9.7 hold carbonated shotcrete layers,

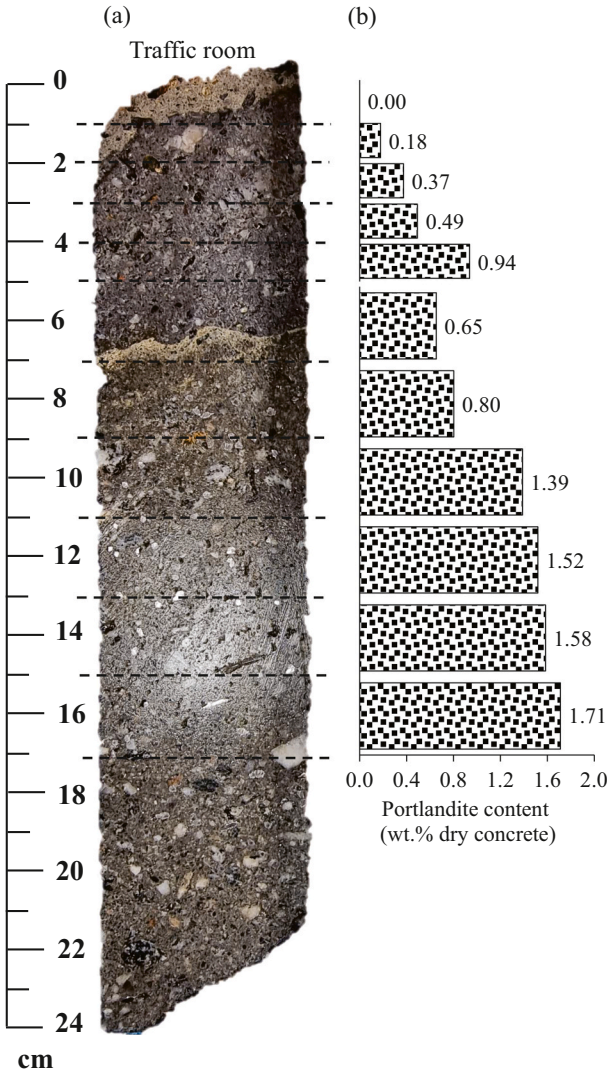

Fig. 14. Portlandite profile in core 2 based on TGA results. (a) Real image of core 2, and (b) portlandite profile discretized every 10 mm in the outermost 5 cm of the shotcrete towards the traffic room and every 20 mm in the following 12 cm.

which do not apparently affect the trend already described.

Suction porosity and density were also measured in cores extracted near the north portal at chainage 8 + 070. Figs. 17 and 18 show the results in core 5 and 7 respectively.

Fig. 17 shows no trend in density and suction porosity towards the traffic room in core 5. Most of the suction porosity values vary between 17 % and 20 % and density values between 2270 and 2320 kg/m^3.

In comparison to core 5, core 7 illustrated in Fig. 18 shows slightly higher suction porosity values between 18 and 21 % and lower density values between mainly between 2250 and 2310 kg/m^3. It is important to highlight as well that the highest suction porosity in cores 5 and 7 occur at the shotcrete surface. A direct comparison between shotcrete density and suction porosity in the two investigated areas in the Frøya tunnel is shown in Fig. 19.

Fig. 19 shows that the highest two suction porosity values and the lowest two shotcrete density values belong to samples from the middle of the tunnel at chainage 5 + 590 near the shotcrete surface.

Profiles of UCS tests with axial deformation along with shotcrete density profiles are shown in Figs. 20 and 21 from cores extracted near the north portal at chainage 8 + 070.

Figs. 20–21 show very similar compressive strength and density results in cores 6 and 8 extracted near the north portal. In particular, UCS strength values exceed 55 MPa in all the cases, while shotcrete density values are always higher than 2280 kg/m^3 with limited scattering in both variables. Note as well that stress strain curves in Figs. 20b and 21b and the failure modes indicate a fragile post-peak behavior in both cases.

Finally, Figs. 22 and 23 show results from the middle of the tunnel at chainage 5 + 590.

Figs. 22 and 23 show compressive strength and shotcrete density reductions towards the traffic room for the cores 10 and 1 extracted from the middle of the tunnel. In both figures, the shotcrete density reduction towards the traffic room is approximately 100 kg/m^3. It is also important to observe that Figs. 22b and 23b describe a different post-peak behavior for the sample closer to the traffic room (samples 1.2 and 10.2) with much gentle peaks in relation to their residual values. A summary of the 8 UCS tests executed in the Frøya tunnel is shown in Fig. 24.

Fig. 24 clearly shows that the lowest compressive strength values (22.5 MPa and 31.7 MPa) are obtained at chainage 5 + 590 in the middle of the tunnel. Figs. 22 and 23 show that these values occur in the samples closest to the shotcrete surface. While the difference between two samples in the cores at chainage 8 + 070 near the north portal is <5 %, the compressive strength reduction towards the traffic room at this location is 35.7 % (31.7 MPa vs 49.3 MPa) in core 10 and 56 % (22.5 MPa vs 51.1 MPa) in core 1. Note that UCS samples 10.2 in Figs. 22 and 1.2 in Fig. 23 have a similar height (8.4 cm and 8.25 cm respectively), and they are both adjacent to the shotcrete surface.

4. Discussion

Leaching is observed in the cores extracted at chainage 5 + 590 (in the middle of the tunnel). This occurs in the outermost 9 cm of the shotcrete towards the traffic room. In this 9 cm, the leaching progressing towards the traffic room was corroborated in the different tests performed, namely, potassium content reduction through μ-XRF (Figs. 9b, 10b), portlandite content reduction through TGA (Fig. 14), suction porosity increase (Fig. 16), shotcrete density reduction (Figs. 16, 22-23), and UCS reduction together with a more ductile behavior (Figs. 22-23). The ingress depth of sulfur and chlorine from the shotcrete surface towards the interior of the shotcrete layer is slightly <9 cm (approximately 7 cm).

On the other hand, there is only a minor indication of leaching at chainage 8 + 070 (near the north portal) within the first centimeter from the shotcrete surface. In this tunnel location, the penetration of chloride and sulfur were only a few millimeters (Fig. 11c and d), the carbonation depth was only a few millimeters (Fig. 8), and the only slightly higher suction porosity values in the two cores analyzed were at the shotcrete surface.

Another interesting difference is the calcium ion concentration measured in the dripping water from the tunnel roof in each of the investigated locations (Table 2). While the calcium ion concentration measured near the north portal was 9 mg/l, the one at chainage 5 + 590 (middle of the tunnel) was 1400 mg/l. The latter value is well above the typical calcium ion concentration in sea water. Thus, the surplus of calcium ion concentration measured at chainage 5 + 590 is very likely related to the decalcification of the shotcrete layer.

One thing in common for the two investigated locations is the formation of a second carbonation layer 7–12 cm away from the shotcrete surface. The carbonation of these layers was identified by the lower pH determined by thymolphthalein, calcite formation in XRD analysis, higher carbonate content in TGA analysis, and higher content of potassium observed through μ-XRF. A possible explanation is that the final shotcrete layer in several stretches of the tunnel was sprayed on long after the previous shotcrete layer, to reinforce specific tunnel stretches after the tunnel breakthrough.

A higher concentration of sulfur in the outermost 7 cm of the

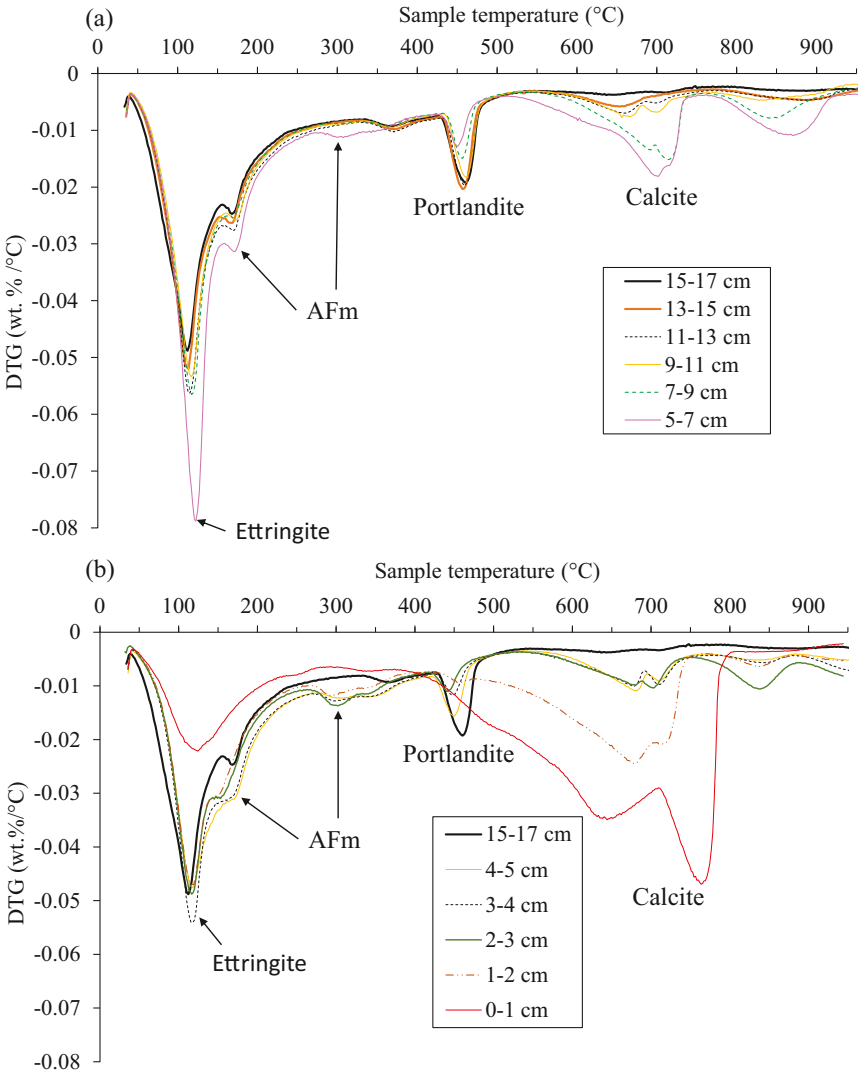

Fig. 15. DTG curves for samples obtained in core 2 at chainage 5 + 590. The legend describes the distance to the shotcrete surface of the sample. (a) From 17.0 cm to 5.0 cm, and (b) from 5.0 cm to 0 cm. The sample "15–17 cm" is repeated in (a) and (b) for easier comparison.

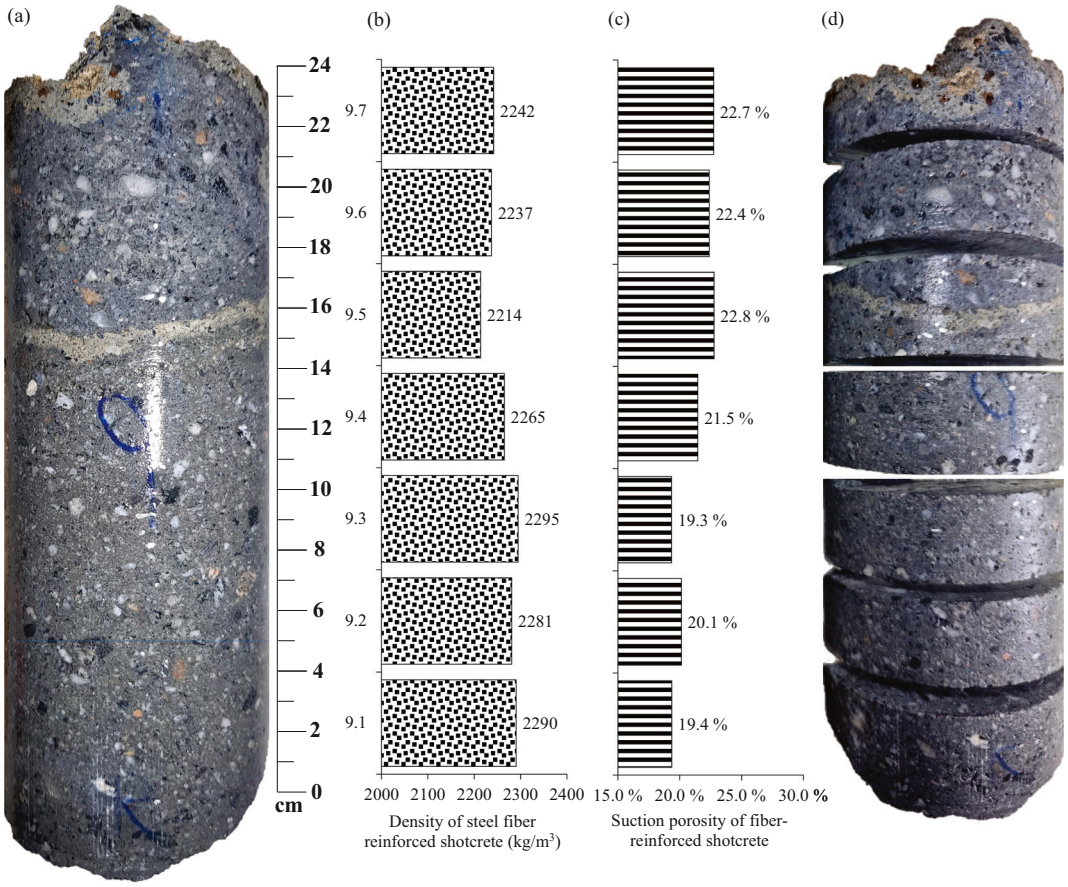

Fig. 16. Profile of suction porosity and density in core 9 (extracted in the middle of the tunnel) split lengthwise. (a) shotcrete core, (b) shotcrete density results, (c) suction porosity results, and (d) actual samples analyzed.

shotcrete at chainage 5 + 590 shown in Figs. 9c and 10c could be explained by saline groundwater running off the shotcrete surface from a higher point in the tunnel. There is no reason to believe that the dosage of alkali-free accelerator was added unevenly when the shotcrete was sprayed. Nevertheless, the higher concentration of sulfur near the shotcrete surface in core 4 (Fig. 11c) obtained from the tunnel location exposed to fresh groundwater at chainage 8 + 070 highlights the role of a sulfur source coming from the traffic room. In the middle of the tunnel, this extra sulfur source for the shotcrete under study would exist in addition to sulfate coming from saline groundwater, and the aluminum sulfate present in the alkali-free accelerator. It is strongly believed that the extra source of sulfur in the traffic room is sulfur dioxide emitted by vehicles.

Saline groundwater running off from a higher spot in the tunnel at chainage 5 + 590 is the probable reason for the chloride ingress observed from the shotcrete surface. Chloride ingress originated from de-icing salts is unlikely in this tunnel location due to the waterproof membrane installed, which hinders a direct exposure of the shotcrete layer with the traffic room. Figs. 9d and 10d show a chloride penetration depth from the shotcrete surface of approximately 7 cm. The TGA results in Fig. 15b indicates the presence of the Friedel's salt in the same zone of the shotcrete layer. Finally, XRD results in Fig. 13 also detected Friedel's salt in a section taken approximately 3 cm away from the shotcrete surface.

Even though actual measurements of groundwater pressure near the rock contour in a typical Norwegian tunnel indicate that it is only a fraction of the total height difference between the groundwater level and the altitude of the specific location in the tunnel [50], it is believed that the hydraulic pressure gradient within the shotcrete layer is higher in the middle of the tunnel than near the portals.

The impression of a lower visibility level experienced in the middle of the tunnel than near the portal leads to believe that a higher air pollution with higher carbon dioxide and sulfur dioxide gas concentrations existed in the middle of the tunnel.

The role of sulfur, chloride and carbon dioxide reacting with the cement paste along with the hydraulic gradient on the leaching level observed in the middle of the tunnel is not disaggregated in this research. The great depth of leaching equal to 9 cm encourages further research on the role of each of them acting separately and in combination.

Finally, it is important to highlight that the 10 shotcrete cores extracted in the Frøya tunnel are only a tiny fraction of the shotcrete volume installed in the whole tunnel, and therefore, general conclusions regarding the shotcrete conditions in this tunnel cannot be established based on this research.

5. Conclusion

The Frøya subsea road tunnel constructed between 1998 and 2000 was inspected in 2021 to determine the extent of the leaching undergone by the steel-fiber reinforced shotcrete used as a single shell rock support in fresh and saline groundwater. Two investigated locations were selected for this purpose. One of the locations is near the north portal where fresh groundwater was found and the other location is in the middle of the tunnel, approximately 150 m below sea level where saline groundwater was identified.

In the middle of the tunnel, the shotcrete layer presented the following figures in the 9 cm closest to the surface exposed to the traffic room:

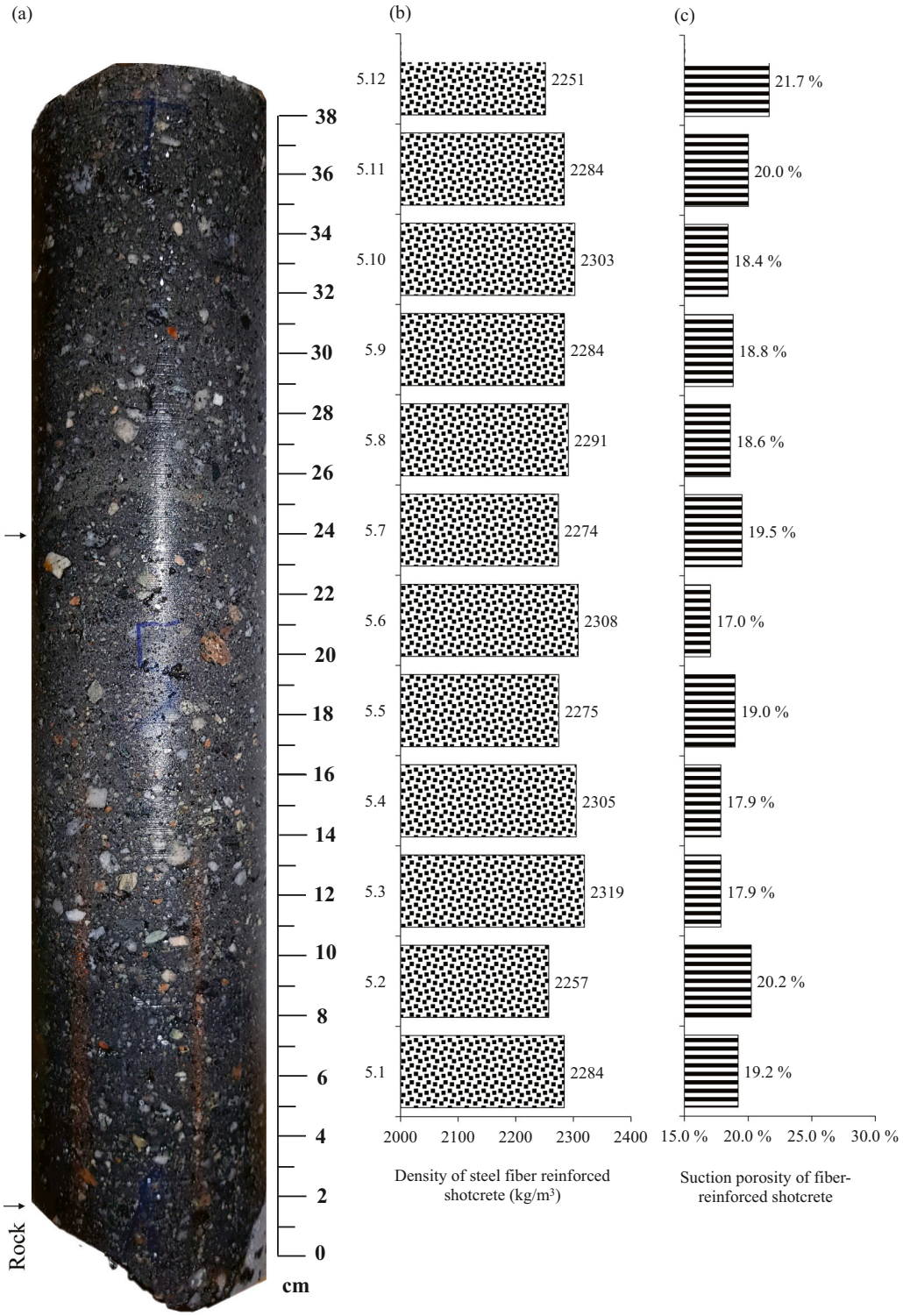

Fig. 17. Profile of suction porosity and density in core 5 extracted near the north portal. (a) shotcrete core, (b) shotcrete density results, and (c) suction porosity results.

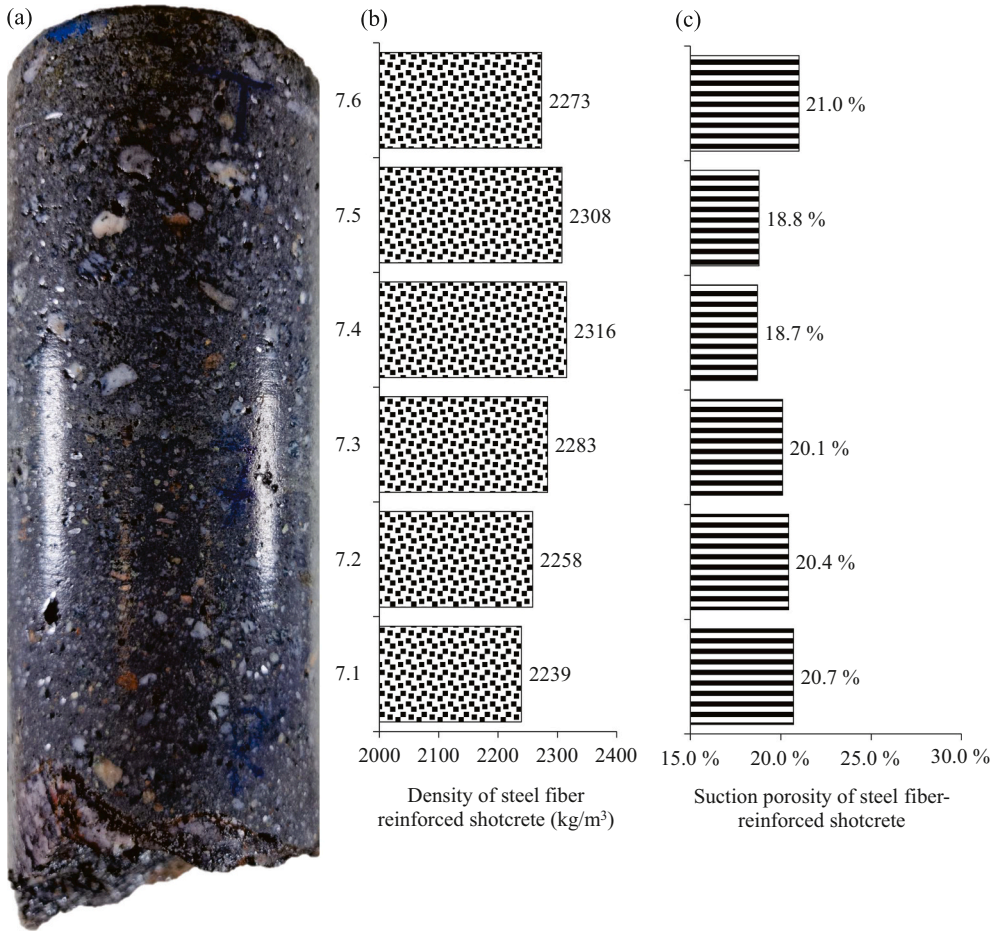

Fig. 18. Profile of suction porosity and density in core 7 extracted near the north portal. (a) shotcrete core, (b) shotcrete density results, and (c) suction porosity results.

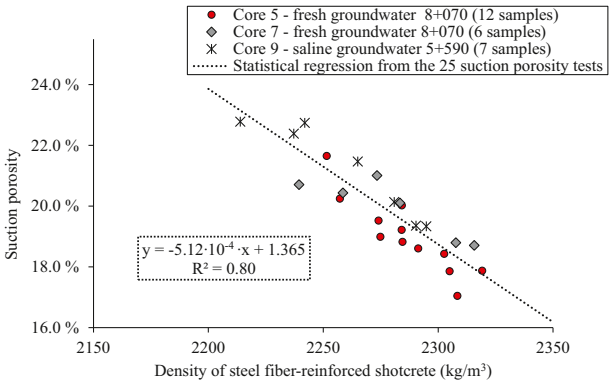

Fig. 19. Correlation between suction porosity and density considering all the samples analyzed in the Frøya tunnel.

- A shotcrete density reduction in the range between 60 kg/m^3 and 103 kg/m^3.
- A reduction in uniaxial compressive strength in the range between 36 % and 56 %.
- In the order of 3 % increase in suction porosity.
- In the order of 68 % reduction in portlandite content through TGA.

Furthermore, the following qualitative observations are highlighted in the same zone of the shotcrete layer:

- An evident reduction in potassium concentration along the cores towards the traffic room through μ-XRF.
- A more ductile post-peak behavior in UCS samples lying adjacent to the traffic room.

All of the abovementioned observations indicate a leaching depth of 9 cm adjacent to the traffic room in the shotcrete installed in the middle of the tunnel. Finally, groundwater chemistry measured in the middle of the tunnel indicates a high concentration of calcium ions dripping from the tunnel roof equal to 1400 mg/l. The latter value, exceeding the typical calcium concentration in sea water of around 400 mg/l, suggests that leaching is occurring by groundwater percolating the shotcrete layer.

As factors that might have influenced this leaching depth observed in the shotcrete installed in the middle of the tunnel, it is highlighted the following:

- Ingress of chlorine and sulfur from the traffic room in the outermost 7 cm of the shotcrete layer.
- Carbonation depth from the shotcrete surface exposed to the traffic room in the order of 1 cm.

Meanwhile, the on-site shotcrete conditions exposed to fresh groundwater near the portal showed:

- There is no apparent trend in potassium concentration along the core.

Fig. 20. Core 6 extracted from chainage 8 + 070 near the north portal. (a) Shotcrete core, (b) stress-strain curve, (c) UCS test results, (d) shotcrete density results, and (e) samples after UCS test completion.

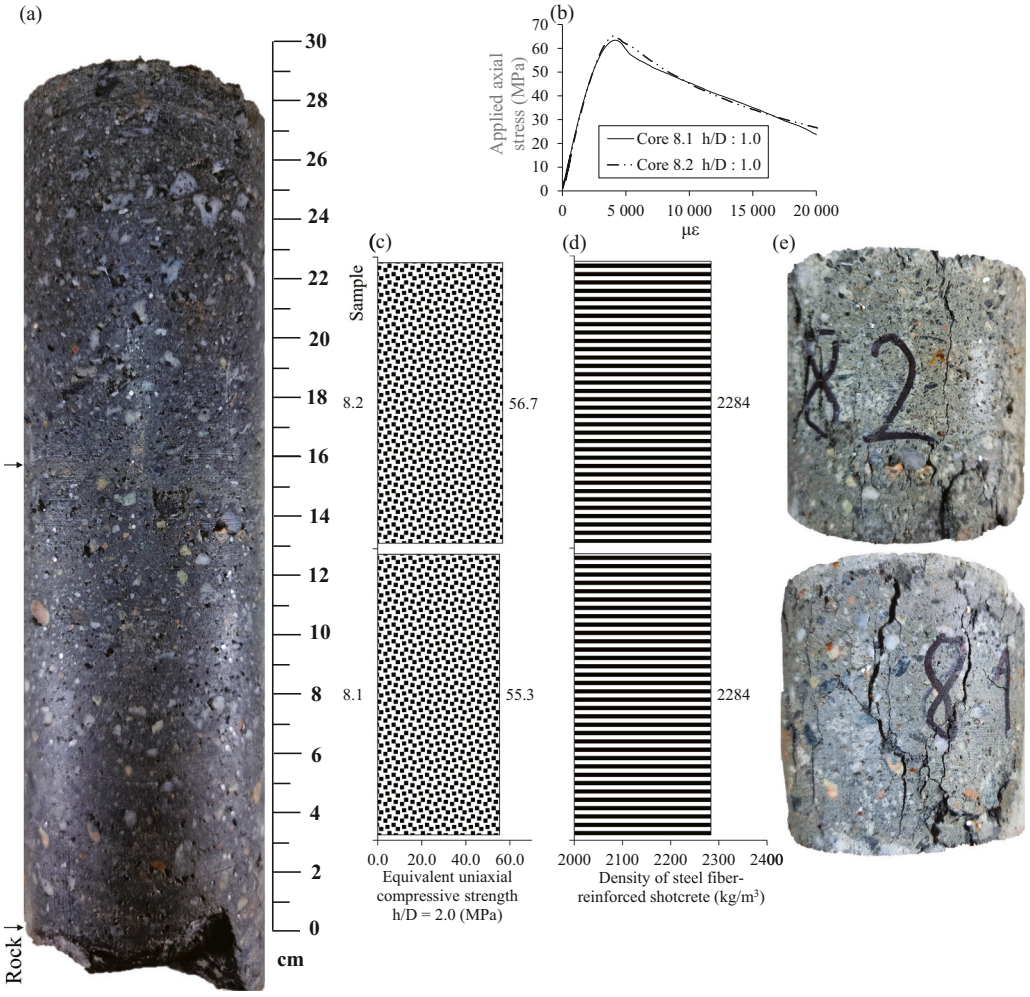

Fig. 21. Core 8 extracted from chainage 8 + 070 near the north portal. (a) Shotcrete core, (b) stress-strain curve, (c) UCS test results, (d) shotcrete density results, and (e) samples after UCS test completion.

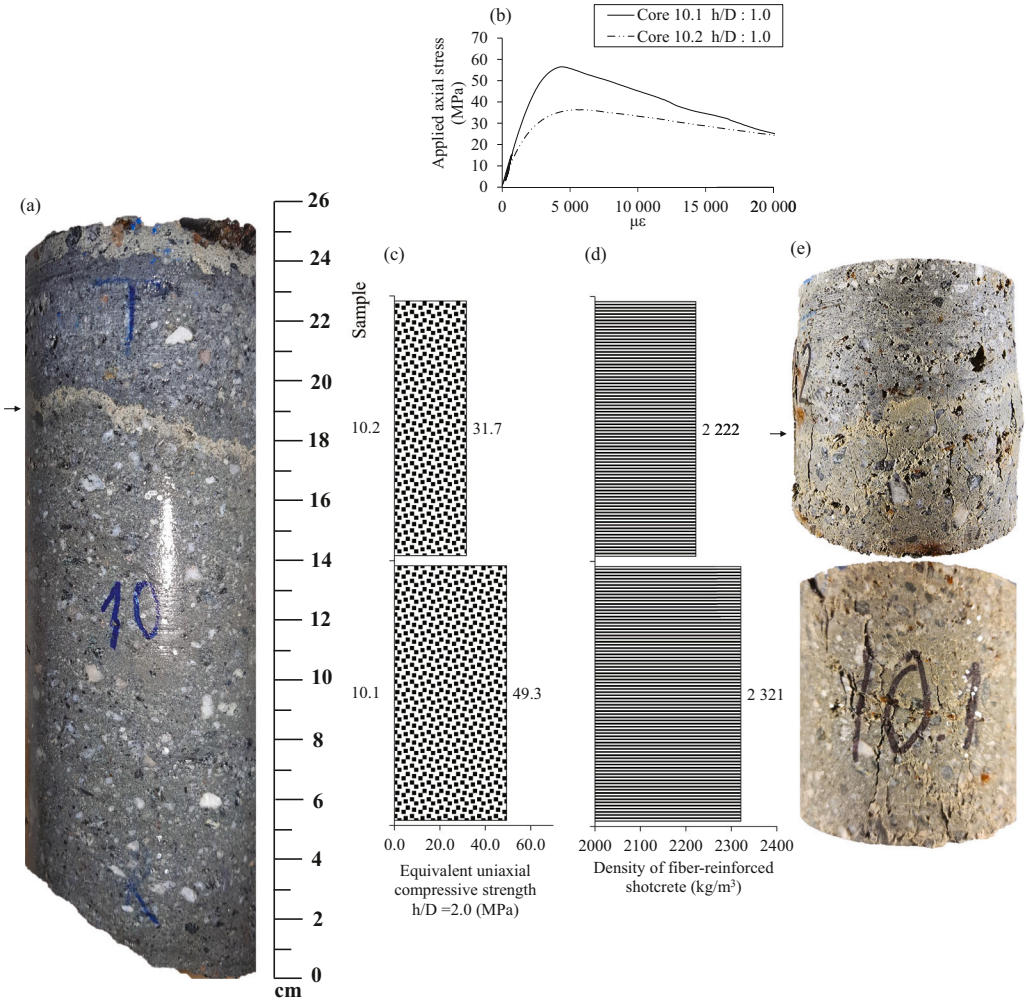

Fig. 22. Core 10 extracted from chainage 5 + 590 (in the middle of the tunnel). (a) Shotcrete core, (b) stress-strain curve, (c) UCS test results, (d) shotcrete density results, and (e) samples after UCS test completion.

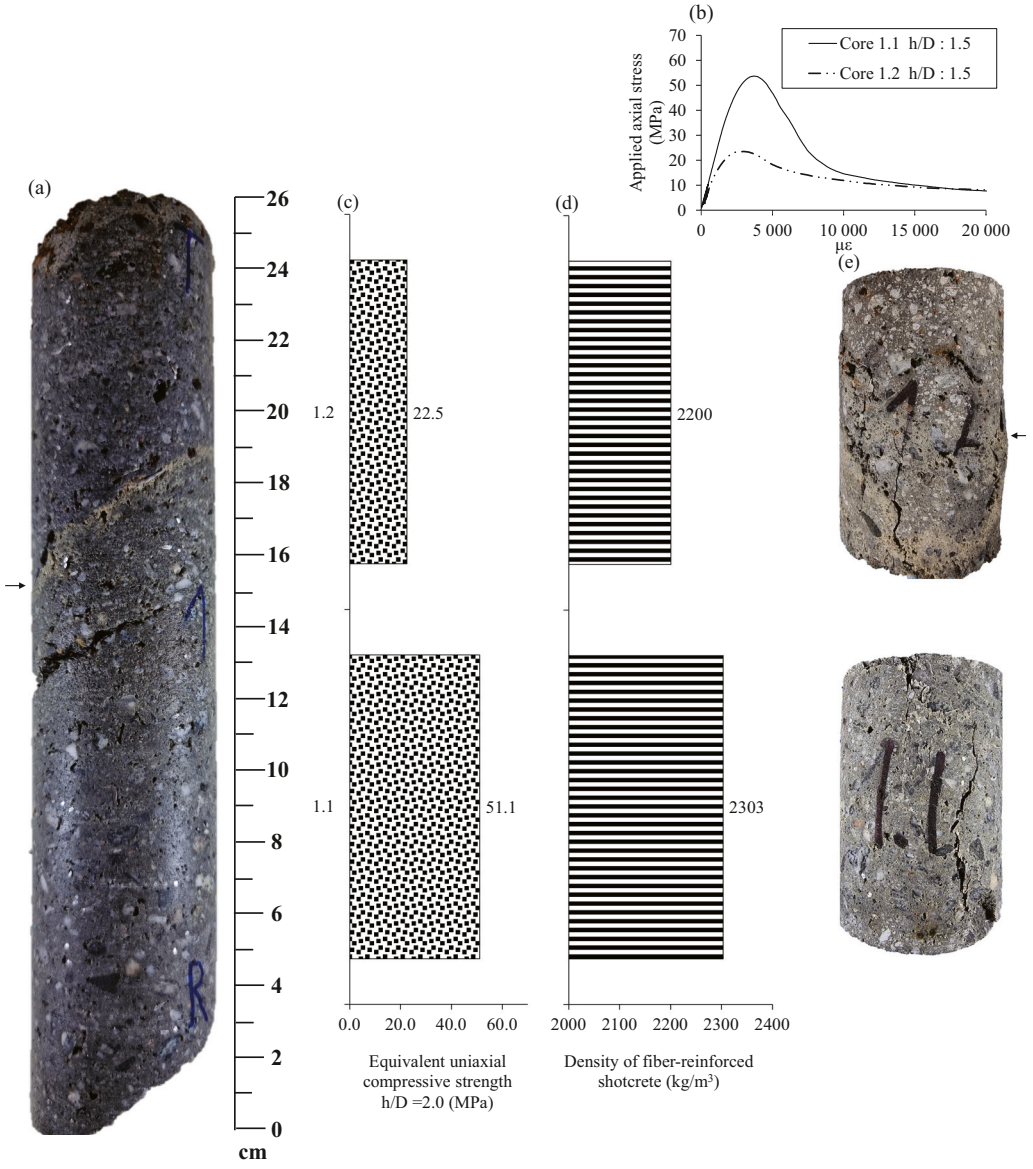

Fig. 23. Core 1 extracted from chainage 5 + 590 (in the middle of the tunnel). (a) Shotcrete core, (b) stress-strain curve, (c) UCS test results, (d) shotcrete density results, and (e) samples after UCS test completion.

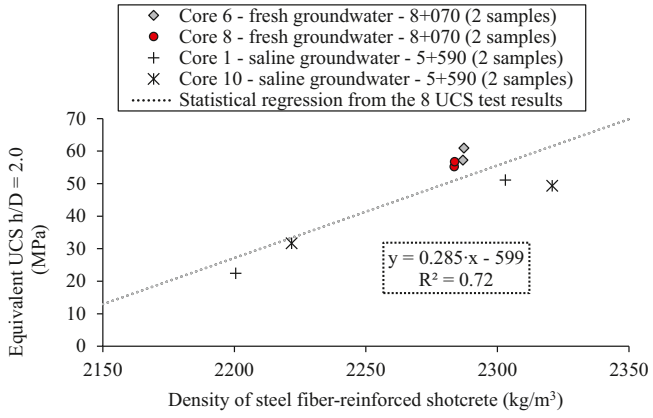

Fig. 24. Correlation between compressive strength and shotcrete density considering the 8 samples analyzed in the Frøya tunnel.

- There is no apparent trend in shotcrete density results along the cores.
- There is no apparent trend in suction porosity results along the cores.
- High compressive strength results with limited scattering and fragile post-peak behavior.
- Low concentration of calcium ions held in groundwater dripping from the tunnel roof (9 mg/l).
- Limited carbonation depth from the shotcrete surface exposed to the traffic room of only a few millimeters.
- Ingress of chlorine and sulfur from the shotcrete surface exposed to the traffic room of only a few millimeters.

The results of the chemical investigations executed in the different cores of the Frøya tunnel lead to believe that the key environmental factors affecting the leaching level observed in the middle of the tunnel are the chemical composition of groundwater containing chlorides and sulfates, the carbon dioxide and sulfur dioxide gas concentrations in the traffic room, and the hydraulic pressure gradient within the shotcrete layer caused by groundwater.

Consent for publication

All authors read and approved the manuscript.

CRediT authorship contribution statement

Cristobal Javier Manquehual: Original draft preparation, Conceptualization, Methodology, Writing, Data curation. **Pål Drevland Jakobsen**: Funding acquisition, Supervision, Reviewing. **Karl Gunnar Holter**: Investigation, Editing, Reviewing. ***Klaartje De Weerdt:*** Editing, Conceptualization, Validation, Reviewing. **Amund Bruland:** Project administration, Supervision.

Declaration of competing interest

Cristobal Javier Manquehual reports financial support was provided by Trøndelag county authority.

Data availability

Data will be made available on request.

References

[1] H. Baji, C.Q. Li, S. Scicluna, J. Dauth, Risk-cost optimised maintenance strategy for tunnel structures, Tunn. Undergr. Sp. Technol. 69 (2017) 72–84, https://doi.org/10.1016/j.tust.2017.06.008.

[2] Y. Yuan, Y. Bai, J. Liu, Assessment service state of tunnel structure, Tunn. Undergr. Sp. Technol. 27 (2012) 72–85, https://doi.org/10.1016/j.tust.2011.07.002.

[3] L. Huang, R.A. Bohne, A. Bruland, P.D. Jakobsen, J. Lohne, Life cycle assessment of norwegian road tunnel, Int. J. Life Cycle Assess. 20 (2015) 174–184, https://doi.org/10.1007/s11367-014-0823-1.

[4] C. Ahn, H. Xie, S. Lee, S. Abourizk, F. Peña-Mora, Carbon footprints analysis for tunnel construction processes in the preplanning phase using collaborative simulation, Construction Research Congress (2010) 1538–1546, https://doi.org/10.1061/41109(373)154.

[5] A. Thomas, N. Chittenden, K.G. Holter, Permanent Sprayed Concrete Linings, 2020. ITA Working Group n°12 and ITAtech.

[6] B. Nilsen, Characteristics of water ingress in norwegian subsea tunnels, Rock Mech. Rock. Eng. 47 (2014) 933–945, https://doi.org/10.1007/s00603-012-0300-8.

[7] E.S. Bernard, Early-age load resistance of fibre reinforced shotcrete linings, Tunn. Undergr. Sp. Technol. 23 (2008) 451–460, https://doi.org/10.1016/j.tust.2007.08.002.

[8] R.P. Salvador, D.A.S. Rambo, R.M. Bueno, S.R. Lima, A.D. Figueiredo, Influence of accelerator type and dosage on the durability of wet-mixed sprayed concrete against external sulfate attack, Constr. Build. Mater. 239 (2020), 117883, https://doi.org/10.1016/j.conbuildmat.2019.117883.

[9] I. Galan, A. Baldermann, W. Kusterle, M. Dietzel, F. Mittermayr, Durability of shotcrete for underground support– review and update, Constr. Build. Mater. 202 (2019) 465–493, https://doi.org/10.1016/j.conbuildmat.2018.12.151.

[10] C. Paglia, F. Wombacher, H. Böhni, M. Sommer, An evaluation of the sulfate resistance of cementitious material accelerated with alkali-free and alkaline admixtures: laboratory vs. Field, Cem. Concr. Res. 32 (2002) 665–671, https://doi.org/10.1016/S0008-8846(01)00739-6.

[11] C. Paglia, F. Wombacher, H. Böhni, The influence of alkali-free and alkaline shotcrete accelerators within cement systems: influence of the temperature on the sulfate attack mechanisms and damage, Cem. Concr. Res. 33 (2003) 387–395, https://doi.org/10.1016/S0008-8846(02)00967-5.

[12] F.R. Steindl, I. Galan, A. Baldermann, M. Sakoparnig, L. Briendl, J. Juhart, M. Thumann, M. Dietzel, R. Röck, W. Kusterle, F. Mittermayr, Sulfate durability and leaching behaviour of dry- and wet-mix shotcrete mixes, Cem. Concr. Res. 137 (2020), 106180, https://doi.org/10.1016/j.cemconres.2020.106180.

[13] J.E. Lien, S. Lillevik, A. Mehlum, S. Soknes, The Frøya tunnel - from geological mapping to completion, 2000. Annual conference of the Norwegian Tunnelling Society (in Norwegian).

[14] B. Gérard, C. Le Bellego, O. Bernard, Simplified modelling of calcium leaching of concrete in various environments, Mater. Struct. Constr. 35 (2002) 632–640, https://doi.org/10.1617/13937.

[15] G. Plusquellec, M.R. Geiker, J. Lindgård, K. De Weerdt, Determining the free alkali metal content in concrete – case study of an ASR-affected dam, Cem. Concr. Res. 105 (2018) 111–125, https://doi.org/10.1016/j.cemconres.2018.01.003.

[16] V. Shah, S. Bishnoi, Carbonation resistance of cements containing supplementary cementitious materials and its relation to various parameters of concrete, Constr. Build. Mater. 178 (2018) 219–232, https://doi.org/10.1016/j.conbuildmat.2018.05.162.

[17] A. Delagrave, M. Pigeon, J. Marchand, E. Revertegat, Influence of chloride ions and pH level on the durability of high performance cement pastes (part II), Cem. Concr. Res. 26 (1996) 749–760.

[18] B. Chen, B. Tian, X. Lu, B. Xiong, Microstructure evolution of leached cement paste: simulation and experiments, Constr. Build. Mater. 231 (2020), 117155, https://doi.org/10.1016/j.conbuildmat.2019.117155.

[19] X.N. Li, X.B. Zuo, Y.X. Zou, Modeling and simulation on coupled chloride and calcium diffusion in concrete, Constr. Build. Mater. 271 (2021), 121557, https://doi.org/10.1016/j.conbuildmat.2020.121557.

[20] W. Müllauer, R.E. Beddoe, D. Heinz, Effect of carbonation, chloride and external sulphates on the leaching behaviour of major and trace elements from concrete, Cem. Concr. Compos. 34 (2012) 618–626, https://doi.org/10.1016/j.cemconcomp.2012.02.002.

[21] A. Machner, M.H. Bjørndal, H. Justnes, L. Hanžič, A. Šajna, Y. Gu, B. Bary, M. Ben Haha, M.R. Geiker, K. De Weerdt, Effect of leaching on the composition of hydration phases during chloride exposure of mortar, Cem. Concr. Res. 153 (2022), https://doi.org/10.1016/j.cemconres.2021.106691.

[22] P. Hagelia, Durability development for sprayed concrete as rock support in different tunnel environments, Norwegian Public Roads Administration (2018). Report No. 566 (in Norwegian).

[23] F.P. Glasser, J. Marchand, E. Samson, Durability of concrete - degradation phenomena involving detrimental chemical reactions, Cem. Concr. Res. 38 (2008) 226–246, https://doi.org/10.1016/j.cemconres.2007.09.015.

[24] Q. Pu, L. Jiang, J. Xu, H. Chu, Y. Xu, Y. Zhang, Evolution of pH and chemical composition of pore solution in carbonated concrete, Constr. Build. Mater. 28 (2012) 519–524, https://doi.org/10.1016/j.conbuildmat.2011.09.006.

[25] T. Van Gerven, G. Cornelis, E. Vandoren, C. Vandecasteele, Effects of carbonation and leaching on porosity in cement-bound waste, Waste Manag. 27 (2007) 977–985, https://doi.org/10.1016/j.wasman.2006.05.008.

[26] P. Hagelia, Deterioration mechanisms and durability of sprayed concrete in Norwegian tunnels, NFF Publication No. 17: Underground openings – operations, maintenance and repair (2008).

[27] R. Ličbinský, J. Huzlík, A. Frýbort, J. Jedlička, K. Kreislová, Specific air pollution in road tunnels, trans, Transp. Sci. 6 (2013) 107–116, https://doi.org/10.2478/v10158-012-0037-9.

[28] R. De Fre, P. Bruynseraede, J.G. Kretzschmar, Air pollution measurements in traffic tunnels, Environ. Health Perspect. 102 (1994) 31–37, https://doi.org/10.1289/ehp.94102s431.

[29] R. Myrdal, Chemical reflections on accelerators for sprayed concrete: Past, present and future challenges, in: 6th Int. Symp. Sprayed Concr. Tromsø, Norway, Sept. 12-15, 2011, 2011. Annual conference of the Norwegian Tunnelling Society (in Norwegian).

[30] C. Javier Manquehual, P. Drevland Jakobsen, K. Gunnar Holter, K. De Weerdt, T. Danner, A. Bruland, Comparison of the condition of steel fiber-reinforced shotcrete with water-glass and alkali-free activators after more than 20 years of service in a subsea road tunnel, Constr. Build. Mater. 328 (2022), 127090, https://doi.org/10.1016/j.conbuildmat.2022.127090.

[31] O.T. Blindheim, E. Grøv, B. Nilsen, Nordic sub sea tunnel projects, Tunn. Undergr. Sp. Technol. 20 (2005) 570–580, https://doi.org/10.1016/j.tust.2005.08.003.

[32] K.H. Holmøy, B. Aagaard, Spiling bolts and reinforced ribs of sprayed concrete replace concrete lining, Tunn. Undergr. Sp. Technol. 17 (2002) 403–413, https://doi.org/10.1016/S0886-7798(02)00065-2.

[33] NPRA, Handbook 021: Road Tunnels, Norwegian Public Roads Administration (in Norwegian) (1992).

[34] NB, Sprayed concrete for rock support. Norwegian concrete association, Publication No. 7 (1993).

[35] K.K. Turekian, Oceans, Prentice-Hall, 1968.

[36] E.D. Goldberg, The oceans as a chemical system, in: The sea, The composition of Sea-Water; Comparative and Descriptive Oceanography, 1963, pp. 3–25. New York.

[37] A.B. Revert, K.De Weerdt, K. Hornbostel, M.R. Geiker, Carbonation Characterization of Mortar with Portland Cement and Fly Ash, Comparison of Techniques, Nord. Concr, 2016. Fed. 1/2016. Publ. No. 54.

[38] F.A. Wahid, PhD Thesis. Characterising Concrete Using Micro X-Ray Fluorescence (μXRF). Department of Civil and Environmental Engineering, Imperial College, London, 2016.
[39] B. Lothenbach, P. Durdziński, K. De Weerdt, Thermogravimetric analysis, in: A Practical Guide to Microstructural Analysis of Cementitious Materials, CRC Press Taylor & Francis Group, 2016.
[40] Sintef, Internal procedure No. KS 70110, Concrete testing. Capillary suction capacity and porosity (1996).
[41] NS-EN 12390–1, Testing hardened concrete Part 1: Shape, dimensions and other requirements for specimens and moulds, 2012.
[42] NS 3420, Description texts for building and construction. Special print on concrete structures., Nor. Counc. Build. Stand. (In Norwegian). (1986).
[43] NS-EN 12390–3: Testing hardened concrete Part 3: Compressive strength of test specimens, 2019.
[44] ISRM, International Society for Rock Mechanics and Rock Engineering, Suggested Methods for Determining Water Content, Porosity, Density, Absorption and Related Properties and Swelling and Slake-Durability Index Properties (1977).
[45] M. Sun, C. Sun, P. Zhang, N. Liu, Y. Li, J. Duan, B. Hou, Influence of carbonation on chloride binding of mortars made with simulated marine sand, Constr. Build. Mater. 303 (2021), 124455, https://doi.org/10.1016/j.conbuildmat.2021.124455.
[46] P. Hemstad, A. Machner, K. De Weerdt, The effect of artificial leaching with HCl on chloride binding in ordinary Portland cement paste, Cem. Concr. Res. 130 (2020), https://doi.org/10.1016/j.cemconres.2020.105976.
[47] A. Gabrisová, J. Havlica, S. Sahu, Stability of calcium sulphoaluminate hydrates in water solutions with various pH values, Cem. Concr. Res. 21 (1991) 1023–1027, https://doi.org/10.1016/0008-8846(91)90062-M.
[48] R.P. Salvador, S.H.P. Cavalaro, I. Segura, A.D. Figueiredo, J. Pérez, Early age hydration of cement pastes with alkaline and alkali-free accelerators for sprayed concrete, Constr. Build. Mater. 111 (2016) 386–398, https://doi.org/10.1016/j.conbuildmat.2016.02.101.
[49] S. Adu-Amankwah, L. Black, J. Skocek, M. Ben Haha, M. Zajac, Effect of sulfate additions on hydration and performance of ternary slag-limestone composite cements, Constr. Build. Mater. 164 (2018) 451–462, https://doi.org/10.1016/j.conbuildmat.2017.12.165.
[50] K.G. Holter, Loads on sprayed waterproof tunnel linings in jointed hard rock: a study based on norwegian cases, Rock Mech. Rock. Eng. 47 (2014) 1003–1020, https://doi.org/10.1007/s00603-013-0498-0.